

We are IntechOpen, the world's leading publisher of Open Access books Built by scientists, for scientists

6,900

Open access books available

185,000

International authors and editors

200M

Downloads

Our authors are among the

154

Countries delivered to

TOP 1%

most cited scientists

12.2%

Contributors from top 500 universities



WEB OF SCIENCE™

Selection of our books indexed in the Book Citation Index
in Web of Science™ Core Collection (BKCI)

Interested in publishing with us?
Contact book.department@intechopen.com

Numbers displayed above are based on latest data collected.
For more information visit www.intechopen.com



Conducting Polymer Nano Composite Epoxy Coatings for Anticorrosive Applications

Gazala Ruhi and S.K. Dhawan

Additional information is available at the end of the chapter

<http://dx.doi.org/10.5772/58388>

1. Introduction

Corrosion is a destructive phenomenon that causes severe damage to metals, alloys, composites etc [12]. The Electrochemical theory of corrosion involves two half-cell reactions, an oxidation reaction at the anode and a reduction reaction at the cathode. For metals corroding in water at neutral pH, the half cell reactions are presented as:

Anodic reaction: $M \Rightarrow M^{n+} + ne^{-}$

Cathodic reaction: $O_2 + 2H_2O + ne^{-} \Rightarrow 4OH^{-}$

These half cell reactions create microscopic anodes and cathodes covering the entire corroding metal surface, which turns to macroscopic anodes and cathodes with the progresses of time. Metals lose their useful properties like metallic lustre, strength, permeability to liquids and gases etc. with prolong exposure to corrosive atmosphere. Mild steel is frequently used as a structural material for marine applications, petroleum production and refining, pipelines, mining etc. because of its good machinability, superior strength and low cost of production. However, this steel is extremely vulnerable towards corrosion. Break down of mild steel occurs, when exposed to diffusive chloride ions, in the sea water. Chromate based conversion coatings were used for many years for corrosion protection of mild steel [3]. These coatings have chromate, an oxidising oxy anion of chromium with superb corrosion resistance. But chromate ion is considered as a serious environmental pollutant and is acutely toxic. As an alternative approach, organic paints and coatings are also applied to protect steel substrates against corrosion [4-8]. But, it is challenging to design corrosion resistant coatings having corrosion protection efficiency equivalent to traditional chromate coatings.

Conducting polymers have attracted immense importance because of their versatile processing applications. These polymers are reported as corrosion inhibitors for active

metals and alloys [9-17]. The mechanism of corrosion protection by conducting polymers involves anodic protection of the underlying metal, by raising its potential to passive region [18]. The polymer exhibits barrier property in its electronically insulating state, where an important feature in its conducting state is the ability to store charge at the metal/coating interface. This charge can be effectively used to oxidize base metal to form a passive layer. Polyaniline and Polypyrrole are the most studied conducting polymers due to their environmental stability, biocompatibility, physical and electrical properties. Polypyrrole is reported as an effective material for corrosion protection purposes [19-23]. Polypyrrole based corrosion resistant coatings can be prepared either by chemical synthesis or it may be electrochemically deposited on the metal surface. Electrochemical deposition of polypyrrole coatings are reported to be carried out on steel substrates using aqueous media [24-30]. These coatings show good adherence to metal surface and thickness of the coatings can be controlled precisely [19-21]. Schaftinghen et.al. have reported that the surface pre-treatment of steel surface prior to electrochemical deposition of polypyrrole coatings has strong influence on corrosion protection performance of the coatings [20]. However, mechanical integrity and thermal stability of coatings in harsh climatic conditions are still questionable. The valuable properties of the coatings lost with prolong exposure to diffusive anions (e.g. chlorides) [31]. To overcome this, conducting polymer based composite systems are interesting alternatives and have attracted substantial academic and industrial interest in recent years. These composites are conducting polymers with thoroughly dispersed small inorganic filler particles. The physical, chemical and mechanical properties of the polymer composites are superior as compared to polymer alone because of the synergistic interaction between the conducting polymers and filler particles [32-39]. Therefore, these composites can be explored as coating material having superior properties. Polyaniline/ SiO_2 composite coatings have been reported to enhance the corrosion resistance of steel substrates [40, 41]. Incorporation of SiO_2 particles as filler in the polymer matrix has shown significant impact on thermal and mechanical properties of coatings [42]. Studies have shown that, silica has a large surface area and smooth non-porous surface [43]. This feature promotes contact between SiO_2 (as filler) and the polymer matrix. In spite of this, the chemically synthesized polymer composites are difficult to apply as coatings because of their non solubility in common organic solvents. Conventional polymer coating like epoxy is known to have superior characteristics as compared to regular paints due to its good scratch resistance and adhesion to metal surface [5-6]. However, epoxy coating alone is not sufficient to protect the underlying metal and fails due to cathodic disbondment under harsh environmental conditions over prolong exposure [44]. Literature shows the use of SiO_2 particles as reinforcement for anti corrosive epoxy coatings [45]. The particles are found to be useful in enhancing properties of organic coatings in aggressive medium [46]. But this effort is not enough for long term corrosion protection of metals. Polymer composites having superior corrosion resistance can be incorporated in the existing epoxy paints to get the desired results. Very limited works are reported on epoxy paints containing polyaniline and polypyrrole as anticorrosive additives [47-49]. In a novel approach, Armelin et.al. [47] have used polyaniline and polypyrrole as additives in epoxy paint system. In this work, it is discussed that the added polymers enhance the corrosion protection ability of

epoxy paint under accelerated conditions and also acts as adhesion promoter. Hema et.al. [99] have studied the corrosion preventive response of polyaniline composites where it has been observed that PANI-SiO₂ composites can be used as effective coatings for corrosion prevention in marine environment.

The crucial question faced by coating industries is to explore green alternatives for chromate conversion coatings with equally good corrosion protection ability. Chitosan is one of the potential candidates for coating purposes with excellent film forming ability, barrier property and affinity towards metals. It is a natural polysaccharide found in the shells of marine crustaceans, a common sea food waste. The proper disposal of the sea food wastes is a continuous problem as it creates major environmental concern associated with ground and drinking water pollution. Chitosan can be explored as an eco-friendly candidate for coating purpose because of its low cost, most plentiful abundance in nature, biodegradable and non-toxic nature [50, 51]. Previous reports have explored the potential use of chitosan coatings for contact lenses and wound dressing [52, 53]. Apart from this, chitosan forms complexes with metal ions and also adheres to negatively charged surfaces. This chemical uniqueness of chitosan can be exploited as corrosion resistant coatings for active metals. A few investigations are carried out to develop chitosan based corrosion resistant coatings for metals [54, 62]. However, chitosan is prone to absorb moisture from atmosphere leading to failure of the coating [63]. A few investigations are carried out to decrease the hydrophilicity and to improve bond strength of chitosan [64, 65]. However, these measures are not sufficient for long term corrosion protection by chitosan coatings. The interaction of chitosan and conjugated polymers like polyaniline, polypyrrole has been reported earlier [66-68]. The synergistic effect of chitosan and polypyrrole is reported to reduce the size and improve the solubility of polypyrrole [69]. The interactive advantage of chitosan and polypyrrole can be used as corrosion resistant coatings for metals like mild steel. In spite of this, the potential of chitosan/polypyrrole composite as a corrosion resistant coating material is not studied well [70].

Present chapter explains the preparation of polypyrrole based nano composite coatings for mild steel substrate using powder coating technique. Powder coating technique is adopted because of the advantage of low cost, excellent finish and almost no emission of volatile organic compounds. The synthesis of polypyrrole/SiO₂ nano composites were carried out using in-situ chemical polymerization of pyrrole monomer on SiO₂ particles. The corrosion protection of the composites was evaluated by Tafel extrapolation, Electrochemical Impedance Spectroscopy (EIS) and salt spray tests in NaCl solution. In order to improve the corrosion resistance of mild steel further, chitosan is introduced in the polymer composite system. Studies are also focussed to highlight the role of chitosan in enhancing the mechanical, thermal and corrosion resistance properties of polypyrrole. SiO₂ particles are purposely added to further enhance the properties of the composite. In order to evaluate the role of chitosan in improving corrosion protection properties, polypyrrole/SiO₂ composites (without chitosan) are also synthesized. The crucial role of SiO₂ is justified by synthesizing chitosan/polypyrrole composites (without SiO₂).

Conducting polymer	Fillers/dopant	Substrates	References/Journal
Polyaniline	a) PO_4^{-3}	mild steel	[39]
	b) SiO_2	mild steel	[40]
	c) TiO_2	steel	[11]
	d) Al_2O_3	carbon steel	[15]
	(e) SiO_2/PFOA	mild steel	[99]
Polyethylene	Ni/Mo	steel	[32]
Polythiophene	-----	steel	[17]
Polypyrrole	a) Diglycidyl ether of bisphenol A (DGEBA)	mild steel	[35]
	b) SO_4^{2-} , pTS ⁻ , DBS	Ni/Ti alloy	[36]
	c) TiO_2	mild steel	[37]
	d) titanate nano tube	stainless steel	[33]
	e) chitosan	steel	[70]

Table 1. Corrosion resistant properties of conducting polymer composites.

2. Electrochemical studies

The electrochemical studies were carried out using Tafel extrapolation method and Electrochemical Impedance Spectroscopy (EIS) in 3.5% NaCl solution at room temperature. Experiments were carried in a conventional three electrode cell assembly using Autolab Potentiostat/Galvanostat, PGSTAT100 (Nova Software). In three electrode cell assembly, the steel strip of dimension 1 cm x 1 cm is taken as working electrode embedded in araldite epoxy, Pt as counter electrode and Ag/AgCl as reference electrode. The surface cleaning of working electrode was carried out by polishing metallographically polishing with 1/0, 2/0, 3/0 and 4/0 grade emery papers. Thereafter, electrodes were thoroughly cleaned with acetone to remove impurities present on the steel surface.

2.1. Tafel extrapolation method

Tafel extrapolation is a method to measure the rate of corrosion, where the working electrode is polarised in positive direction from cathodic to E_{corr} ending at anodic to E_{corr} . Figure 1 shows the potential vs. log current plot for an applied potential scan.

The anodic and cathodic curves are drawn by running the test results using electrochemical software. The anode is polarised upwards to more positive values by an amount η_a (anodic polarisation). Whereas, the cathode is polarised downwards to a more negative value by an amount η_c (cathodic polarisation). Here, η is over voltage (measure of polarisation with respect to equilibrium potential of an electrode). The measured electrode potential is called as corrosion (E_{corr}). The point of intersection between the two rectilinear polarisation curves in

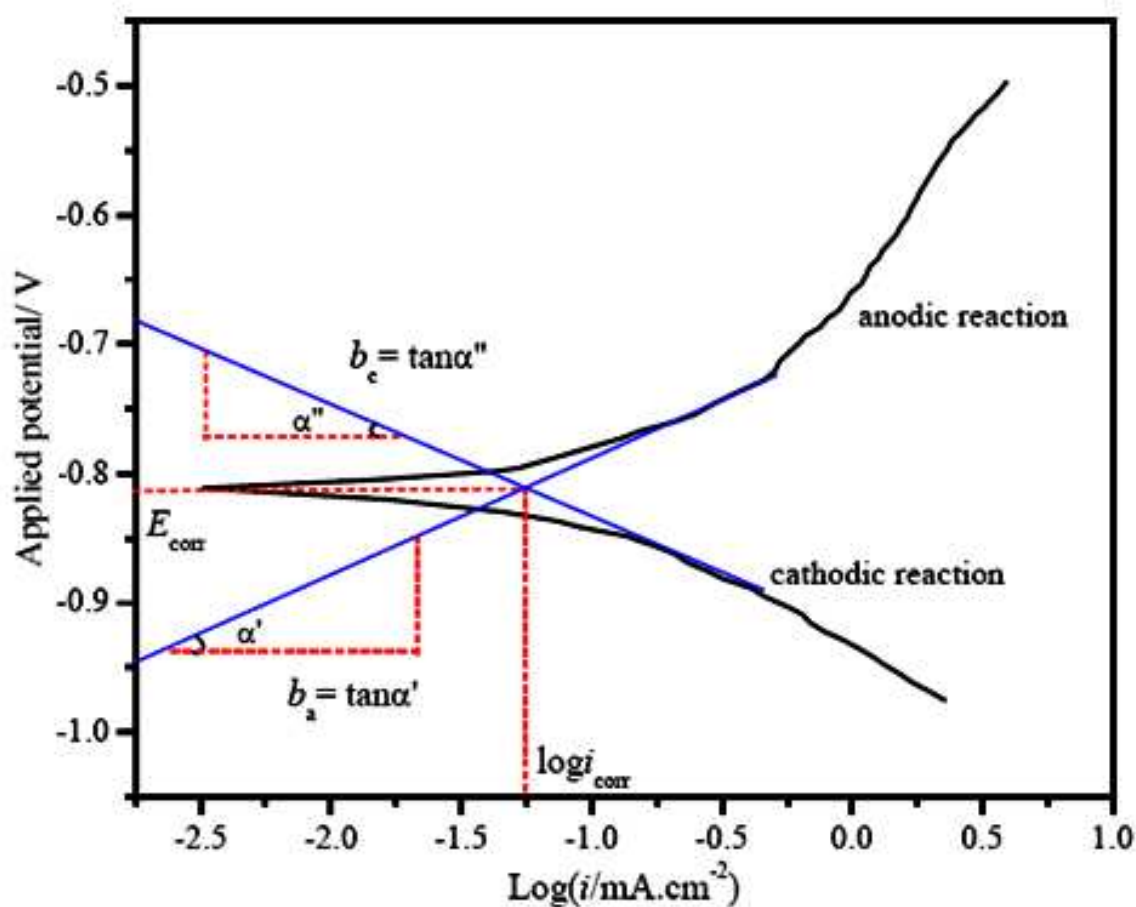


Figure 1. Polarisation curve of a corroding metal using Tafel extrapolation

the polarisation diagram (Figure 1) gives the value of corrosion current (i_{corr}). The values of anodic (β_a) and cathodic (β_c) Tafel constants are measured from the anodic and cathodic slopes respectively. It is possible to measure corrosion rate (C.R) in mm/year by knowing the value of i_{corr} using equation 1.

$$\text{C.R} = 3.268 \times 10^3 \times \frac{i_{\text{corr}}}{\rho} \frac{\text{MW}}{z} \quad (1)$$

Where MW is the molecular weight of the specimen (g/mole), ρ is density of the specimen (g/m³) and z is the number of electrons transferred in corrosion reactions.

2.2. Electrochemical Impedance Spectroscopy (EIS)

Electrochemical impedance spectroscopy (EIS) is a non-destructive technique which gives accurate kinetic and mechanistic information of a corroding system [71-79]. It is one of the powerful tools to study the corrosion rate. The impedance technique has been widely used to extract information concerning the interaction of metal/coating system with the corrosive environments, degradation of highly resistive organic coatings [80-83], corrosion rates at the

defects and porosity in the coating. The impedance data is measured from Nyquist and Bode plots. Nyquist plot is also known as Cole-Cole plot (Figure 2a). In this plot, the real part of impedance $Z' = |Z| \cos \phi$ and imaginary part $Z'' = |Z| \sin \phi$ of the impedance is plotted against each other at each excitation frequency. Usually the plot of Z' vs Z'' is a semicircle and it cuts the Z' axis at high frequency corresponding to R_s (solution resistance) and at low frequency corresponding to $R_s + R_{ct}$. Kinetic parameters like R_s , R_{ct} (charge transfer resistance) and C_{dl} (double layer capacitance) can be calculated from Nyquist plot. The disadvantages of the Nyquist plot are that the frequency does not appear explicitly and capacitance of the electrode can be calculated only after knowing the frequency. In Bode plots (Figure 2b), impedance ($\log Z$) and phase angle (ϕ) are plotted against log of frequency. Bode plots give the information regarding the variation of impedance with respect to the frequency.

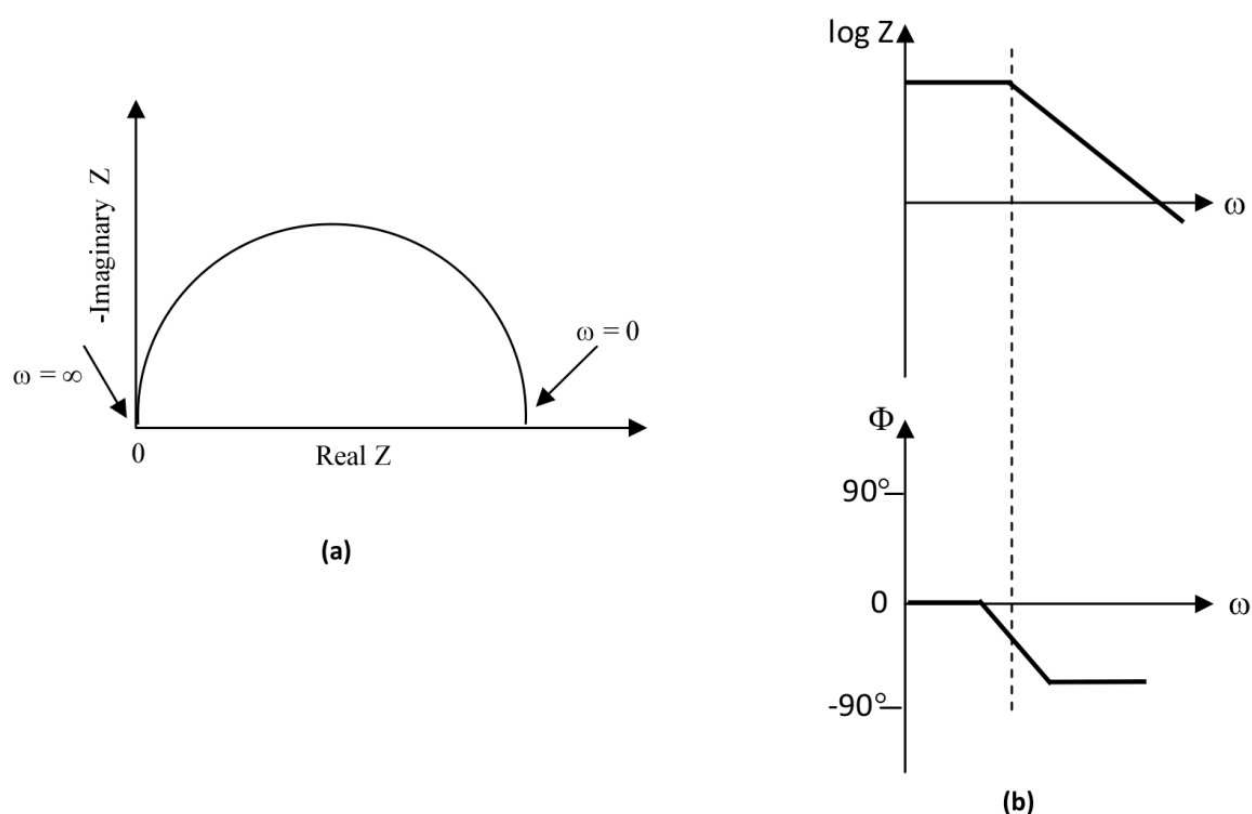


Figure 2. (a) Nyquist plot showing real vs imaginary part of impedance. (b) Bode plots showing the variation of impedance ($\log Z$) and phase angle (Φ) with respect to change in frequency

2.3. Salt spray fog test

The salt spray fog test is a standardized method used to check corrosion resistance of coatings exposed to aggressive environments. Salt spray test is an accelerated corrosion test that produces a corrosive attack to the coated samples in order to predict their corrosion tolerance under high salt and humidity conditions. An intentional scribe mark is applied on the coated

surface and the appearance of corrosion products (oxides) is evaluated after a period of time. Test duration depends on the corrosion resistance of the coatings. Salt spray test is popular because it is cheap, quick, well standardized and reasonably repeatable. Salt spray test is widely used in the industrial sector for the evaluation of corrosion resistance of coated surfaces or parts. The apparatus for testing consists of a closed testing chamber, where a salted solution (mainly, a solution of 5% NaCl) is atomized by means of a nozzle. This produces a corrosive environment of dense saline fog in the chamber so that parts exposed in it are subjected to severely corrosive conditions. Chamber construction, testing procedure and testing parameters are standardized under national and international standards, such as ASTM B 117 and ISO 9227. These standards contain the necessary information regarding testing parameters like temperature, air pressure of the sprayed solution, preparation of the spraying solution, concentration, pH, etc. Different coatings have different behaviour in salt spray test and consequently, test duration will differ from one type of coating to another.

3. Experimental work

3.1. Synthesis SiO₂ particles

The synthesis of mono disperse uniform sized SiO₂ particles was carried out by hydrolysis of tetra-ethyl orthosilicate (TEOS, Merck) in ethanol using ammonia as a catalyst. Aqueous ammonia (3.14ml, Merck) was added to a solution of ethanol in water. The solution was vigorously stirred for 1 hr. To this, 5 ml of TEOS was added slowly with constant stirring for the proper hydrolysis of TEOS. The appearance of turbidity indicated the formation of SiO₂ particles. The particles were retrieved by centrifuging at 15000 rpm for 5 minutes. The obtained powder was calcined at 600°C in a furnace. The calcined silica was crushed by mortar pastel and kept in a desiccator for further use.

3.2. Synthesis of polymer composites (Polypyrrole/SiO₂)

Polypyrrole/SiO₂ composites (PCs) were synthesized by chemical oxidative polymerization of pyrrole (Acros Organics) using ferric chloride as an oxidant [84]. The schematic view of the synthesis is shown in Figure 3. Pyrrole and silica were taken to a weight ratio of 3:1 to form the composite. For this, synthesized SiO₂ particles were dispersed in deionised water using a mechanical stirrer. 0.01 M of sodium lauryl sulphate (SLS) was added to the above suspension with continuous stirring. Thereafter, 0.1 M of pyrrole was added slowly followed by drop wise addition of ferric chloride solution (0.1M). The appearance of black colour showed the start of polymerization of pyrrole. The polymerization was carried out at room temperature for a period of 4-5 hrs. The synthesized polymer composites (PCs) were retrieved from the suspension using G 4 filtration funnel. The obtained powder was washed with deionised water several times to remove oxidant and oligomers, followed by drying in a vacuum oven at 60°C.

3.3. Preparation and deposition of powder coating

The polymer composite (PCs) was blended with epoxy powder coating formulation in various wt% loadings (1.0, 2.0, 3.0 and 4.0%) using a laboratory ball mill. For epoxy powder coating formulation has following composition: resin {epoxy (bisphenol A)+polyester} (70%), Flow agent (D-88) (2.3%), degassing agent (benzion) (0.7%), fillers (TiO_2 and BaSO_4) (27%). A homogenous mixture of well dispersed PCs in epoxy was obtained after ball milling. The blended epoxy-polymer composite formulation was applied on mild steel specimens using an electrostatic spray gun held at 67.4 KV potential with respect to the substrate. The powder coated mild steel specimens were cured in oven at 180°C for 30 minutes. The adhesion of the coatings was tested by tape test as per ASTM D3359-02 and found to pass the test.

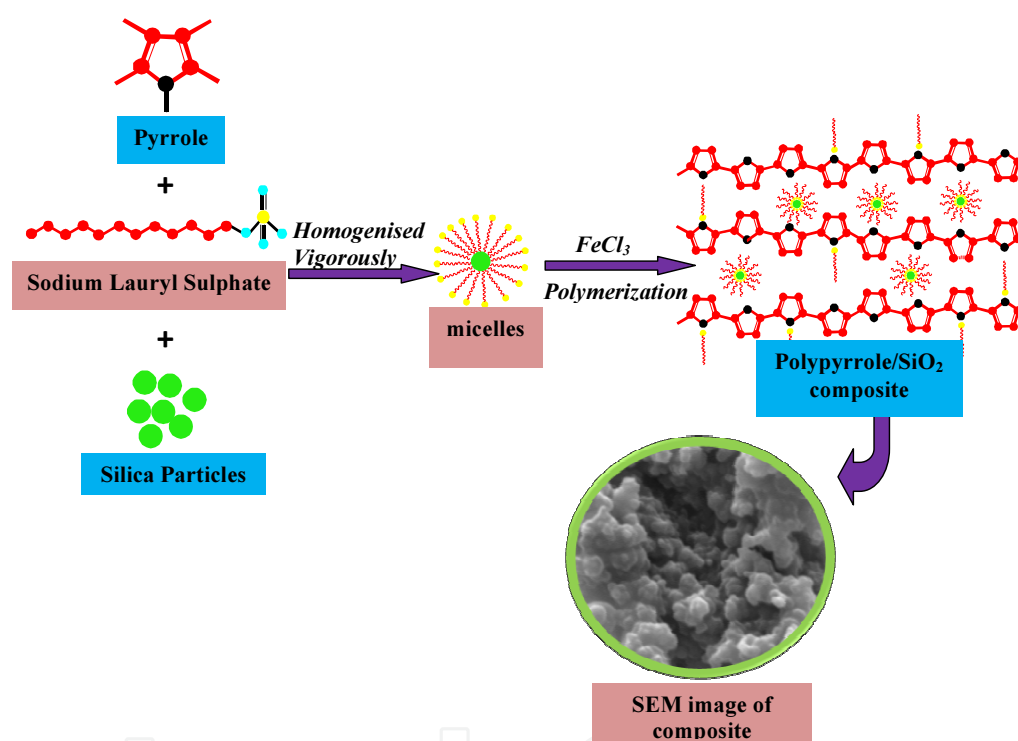


Figure 3. Schematic diagram of the synthesis of the polypyrrole/SiO₂ composite. (Progress in Organic Coatings DOI: 10.1016/j.porgcoat.2014.04.013).

4. Characterization of polypyrrole/SiO₂ composite

4.1. FTIR spectra

Figure 4 shows the FTIR spectra of SiO₂, polypyrrole alone and polypyrrole/SiO₂ composite (PCs). The FTIR spectrum of SiO₂ exhibits the characteristic bands of stretching and bending vibration of Si-O-Si at 1108 and 817 cm⁻¹, respectively. In FTIR spectrum of polymer composite, the observed peak at 1554 cm⁻¹ corresponds to typical pyrrole ring vibration [85]. The low

intensity peak at 1474 cm^{-1} is attributed to =CH in plane vibrations and the peak at 771 cm^{-1} is due to =CH out of plane vibrations [86-88]. A peak of considerable intensity at 1038 cm^{-1} is the N-H in plane deformation absorption of polypyrrole. The corresponding peak of C-N stretching [89] of polypyrrole at 1186 cm^{-1} is masked by a band (at 1108 cm^{-1}) of SiO_2 . For polypyrrole alone, the characteristic peaks of pyrrole rings, in and out of plane =CH vibrations are observed at 1559 , 1480 , 929 and 789 cm^{-1} , respectively [90]. On comparing the peaks of polypyrrole alone and polymer composites (PCs), it is observed that shifting of FTIR peak of polypyrrole occurred as a result of the incorporation of SiO_2 particles in the polymer matrix (Figure 4). The =CH out of plane vibration at 789 cm^{-1} of polypyrrole alone is shifted to a lower wave number (771 cm^{-1}) for the composite. The appearance of a broad band at 3440 cm^{-1} for the polymer composite (PCs) may be attributed to the interaction between SiO_2 and polypyrrole through hydrogen bonding between proton on N-H and oxygen atom on SiO_2 . The above results show a strong interaction between polypyrrole and SiO_2 particles of the composite.

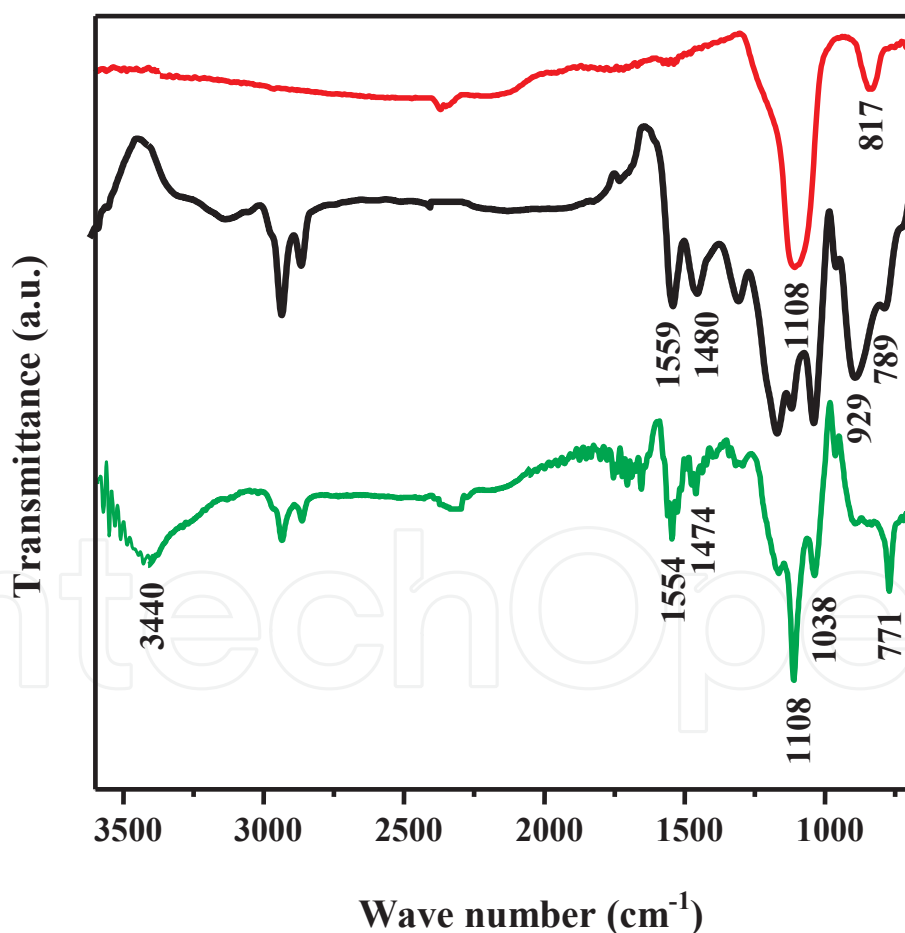


Figure 4. FTIR spectra of SiO_2 (—), polypyrrole alone (—), and polypyrrole/ SiO_2 composite (—). (Progress in Organic Coatings DOI: 10.1016/j.porgcoat.2014.04.013).

4.2. X-ray diffraction

Figure 5 shows the XRD powder diffraction pattern of SiO_2 and polymer composite. One can find a broad diffraction peak at 2θ of 24.3° corresponding to the semi crystalline nature of synthesized SiO_2 particles. For polypyrrole/ SiO_2 composite, the broad characteristic peak has shifted to 22.2° . The shifting may be due to the SiO_2 particles embedded in the polymer matrix. A uniform covering of amorphous polypyrrole on the surface of SiO_2 is expected.

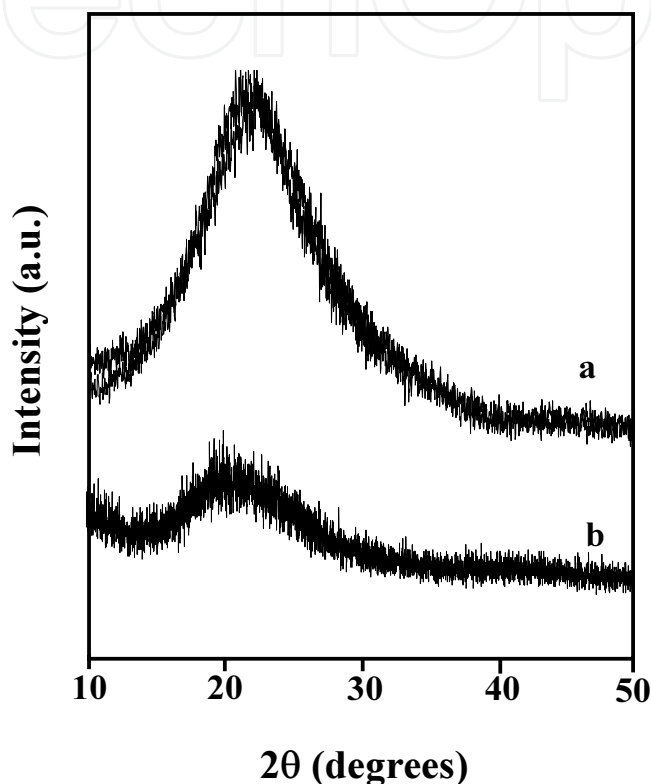


Figure 5. XRD graphs of (a) SiO_2 and (b) polypyrrole/ SiO_2 composite. (Progress in Organic Coatings DOI: 10.1016/j.porgcoat.2014.04.013).

4.3. Thermo Gravimetric Analysis (TGA)

The thermogravimetric profiles of SiO_2 , polypyrrole alone and polymer composite (PCs) are presented in Figure 6. The thermograms were recorded by heating the samples at a temperature range of 25 to 600°C under nitrogen atmosphere (60 ml/min). As shown in Figure 6, the SiO_2 particles are found to be thermally stable with almost no weight loss over the entire range of temperature. The thermogram of polypyrrole alone indicates three stage weight loss. In the first stage, 5-6% weight loss at temperature 100°C is attributed to the loss of water molecules from the polymer matrix [91]. The weight loss at second stage that starts above 100°C until 220°C (about 7-8%) is basically due to the removal of dopants and low molecular weight oligomers. The gradual weight loss above 250°C represents the thermal decomposition of polypyrrole backbone [92]. The thermogram of polymer composite exhibits a three stage

weight loss pattern similar to polypyrrole alone. It exhibits an initial weight loss of 6% (around 100°C) due to loss of residual water molecules followed by 7% weight loss (around 230°C) due to removal of dopants and oligomers. However, a considerable enhancement in the thermal stability is noticed for the polymer composite. With the addition of SiO₂, the thermal decomposition of polypyrrole (250°C) increases to 330°C for the polymer composite. The improvement in the thermal stability of the composite is certainly attributed to the presence of SiO₂ as filler. SiO₂ is stable in the range from room temperature to 600°C, when combined with polypyrrole, it restricts the thermal motion of the polypyrrole chains and shields the degradation of polymer [93]. The retarding effect of SiO₂ on the movement of polypyrrole chains also shows the relatively compact structure of polypyrrole/SiO₂ composite. The weight loss for polypyrrole alone and polymer composite at 600°C is found to be 63% and 57%, respectively. The decrease in weight loss indicates the interaction of polypyrrole with SiO₂ particles.

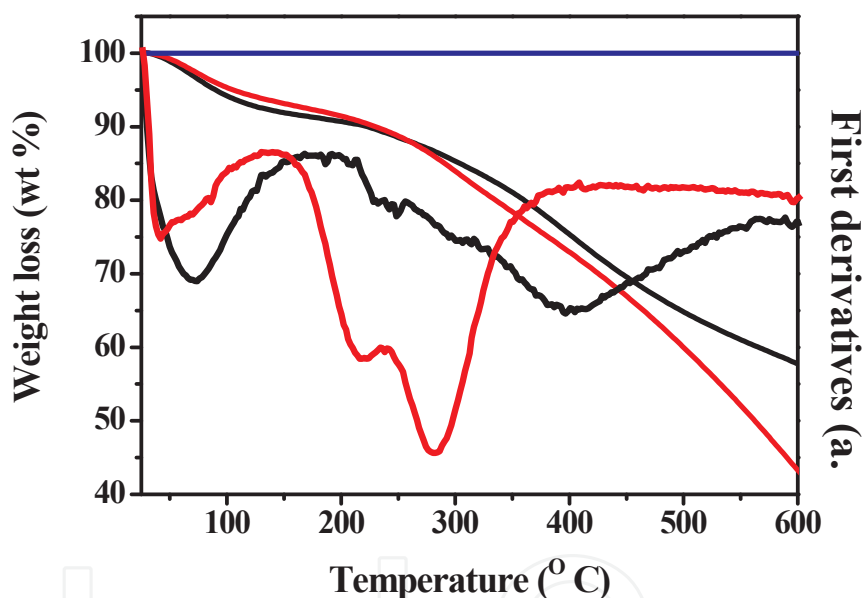


Figure 6. TGA graphs of SiO₂ (—), polypyrrole alone (—) and polypyrrole/SiO₂ composite (—). Their first derivatives are also shown here. (Progress in Organic Coatings DOI: 10.1016/j.porgcoat.2014.04.013).

4.4. SEM/TEM micrographs

Figure 7a depicts the scanning electron micrograph of synthesized SiO₂ particles. The particles exhibit spherical morphology with smooth texture. The average particle size of SiO₂ is 200 nm. The microstructural features of polymer composite (PCs), as shown in Figure 7b reveal a globular cluster of polypyrrole matrix incorporating SiO₂ particles. The entrapment of SiO₂ particles in the matrix can easily be noticed in Figure 7b. EDX analysis shows the presence of elements, Si (51.74%) and O (10.49%) from SiO₂, C (33.61%) and N (1.28%) from polypyrrole in the composite. The TEM image of polymer composite is shown in Figure 7c. It can be noticed

that majority of SiO_2 particles are covered with polypyrrole. Some free separated SiO_2 particles can also be seen in the micrograph (Figure 7c). The SiO_2 particles are found to be well dispersed in polymer matrix. The large contact area of SiO_2 and polypyrrole in the polymer composite resulted in a more uniform composite structure. The microstructural analyses are in good agreement with FTIR and XRD results of polymer composite, confirming a strong interaction between polypyrrole and silica in the composite.

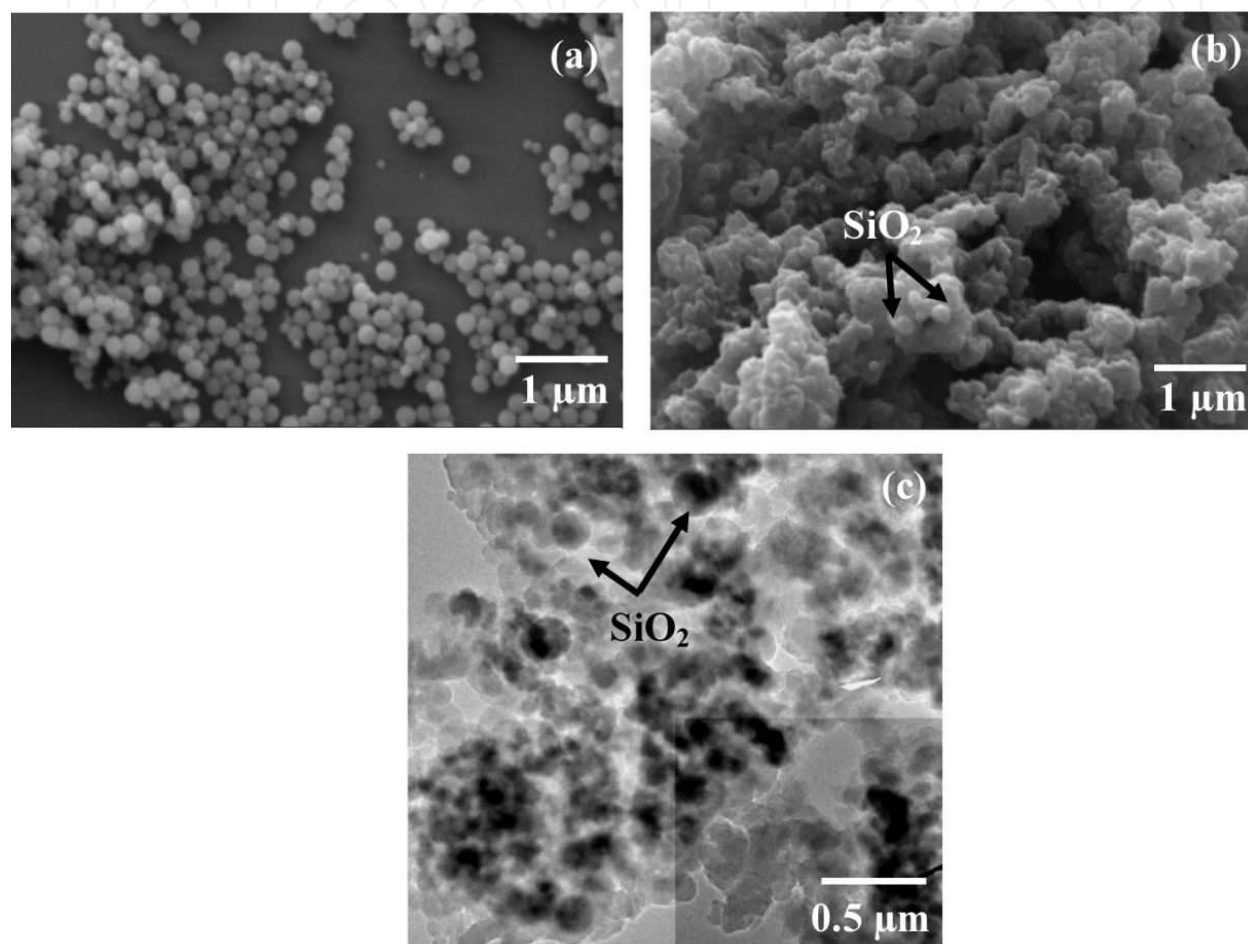


Figure 7. SEM micrographs showing morphology of (a) SiO_2 particles, (b) polypyrrole/ SiO_2 composite. SiO_2 particles embedded inside the polymer matrix are visible in the micrograph. (c) TEM micrograph of polypyrrole/ SiO_2 composite showing even distribution of SiO_2 particles in the composite. (Progress in Organic Coatings DOI: 10.1016/j.porgcoat.2014.04.013).

4.5. Corrosion studies of polymer composites in 3.5% NaCl solution

4.5.1. Tafel polarization

Figure 8 shows the Tafel polarisation behaviour of epoxy coated (EC) and epoxy with different wt% loading of polymer composites (PCs) coated steel specimens (PCs1, PCs2, PCs3 and PCs4) in 3.5% NaCl at room temperature ($25 \pm 3^\circ\text{C}$). The plots were drawn to derive the values of

different electrochemical parameters like corrosion potential (E_{corr}), corrosion current density (i_{corr}), anodic (β_a) and cathodic (β_c) Tafel constants. i_{corr} , β_a and β_c are measured by extrapolating the anodic and cathodic curves using Tafel extrapolation method (Table 1). The variability in the test results was found to be 2-3% for each measurement. Figure 8 exhibits a remarkable shift of E_{corr} towards positive potential for the epoxy with different wt% loading of PCs coated steel specimens as compared to the epoxy coated (EC) steel specimen. One can notice a slight reduction in E_{corr} for epoxy with 1 wt% loading of polymer composite coated steel specimen (PCs1) as compared epoxy coated steel (EC) specimen. However, the measured E_{corr} is found to be significantly increased for steel specimens coated with 2-4 wt% loading of polymer composite in epoxy. The E_{corr} occurred 177, 554 and 667 mV vs Ag/AgCl more positive for specimens PCs2, PCs3 and PCs4, respectively than the specimen EC (Table 1). The more positive values of E_{corr} for the epoxy with PCs coated specimens indicate the presence of a passive layer on the metal surface that control the anodic/cathodic reactions. The corrosion current density (i_{corr}) of epoxy coated steel specimen (Table 1) is observed to be eight times less than the bare mild steel (not shown here). Conventional polymeric coatings like epoxy are known to have good resistance towards diffusive ions and long exposure time is required to evidence degradation of polymeric chains [94]. The i_{corr} further reduced significantly with the addition of polymer composite in the epoxy resin. The trend of decrease of i_{corr} is in accordance with the increase of wt% loading of polymer composite in epoxy. The i_{corr} of PCs1 occurred four times less than the specimen EC. For specimens PCs2, PCs3 and PCs4, the measured i_{corr} is found to be two, more than four and four orders of magnitude less, respectively as compared to the specimen EC (Table 1). The significant reduction in the values of i_{corr} for the epoxy with polymer composite coated steel specimens indicate the effective corrosion protection performance of the polypyrrole/SiO₂ composite when added as additive in the epoxy resin. Further, the occurrence of notably higher value of anodic and cathodic Tafel constants for epoxy with polymer composite coated steel specimens as compared to epoxy coated specimens implies the effective role of polymer composite in controlling anodic and cathodic reactions. The combined effect of presence of conjugation in the polymer backbone and the presence of polar N-H group in the pyrrole ring acts as corrosion inhibitor [95]. Additionally, polypyrrole facilitates delocalisation of charge through it, which hinders the formation of localised anodic and cathodic currents. This ultimately makes the coated surface resistant towards corrosion that requires localization of charges [95]. Previous works carried out by Wessling [96], Sathiyarayanan et al. [97], Nguyen et al. [98] and Hema et. al. [99] explain the ability of conducting polymers to intercept electrons at metal surface and transport them. Similarly, works on PANI/SiO₂ composite in epoxy coatings also It is important to note that the epoxy with 4.0 wt% loading of PCs coated specimen (PCs4) exhibits more positive E_{corr} as compared to the epoxy with 3.0 wt% loading of PCs coated specimen (PCs3). But interestingly, the i_{corr} for specimen PCs3 is observed to be less than the specimen PCs4. This shows the better corrosion resistance of epoxy coating with 3.0 wt% loading of PCs. This could be the optimum limit of loading of PCs in the epoxy system.

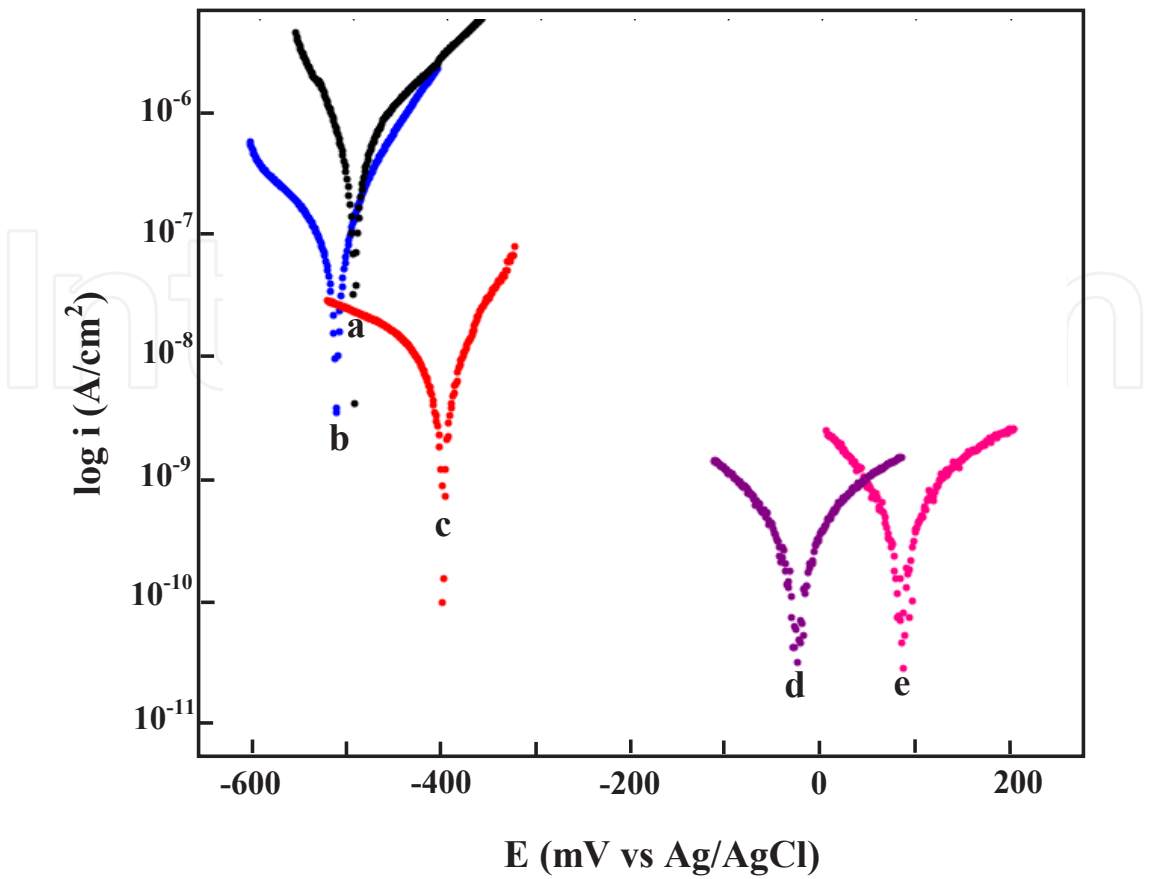


Figure 8. Tafel plots of (a) epoxy coated and epoxy with (b) 1.0 wt%, (c) 2.0 wt%, (d) 3.0 wt% and (e) 4.0 wt% loading of polypyrrole/SiO₂ composite (PCs) coated mild steel specimens in 3.5% NaCl solution at room temperature (25+3°C). (Progress in Organic Coatings DOI: 10.1016/j.porgcoat.2014.04.013).

Sample Name	Loading level of composite	E _{corr} (mV)	i _{corr} (A/cm ²)	β _a (mV/decade)	β _c (mV/decade)
EC	-----	-582.4	8.4x10 ⁻⁷	92.1	189.8
PCs1	1.0 wt%	-523	1.9x10 ⁻⁷	333.6	97.9
PCs2	2.0 wt%	-405.3	1.8x10 ⁻⁸	659.4	126.7
PCs3	3.0 wt%	-28.3	1.3x10 ⁻⁹	408.7	603.5
PCs4	4.0 wt%	83.5	1.5x10 ⁻⁹	285.1	441.7

Table 2. Different electrochemical parameters obtained by Tafel extrapolation for epoxy and epoxy with different wt % loading of polymer composite in 3.5% NaCl solution.

The polarisation resistance (R_p) is inversely related to corrosion current density (i_{corr}) through Stern-Geary equation [100] as mentioned in equation 2.

$$R_p = \frac{\beta_a \beta_c}{2.3.3(\beta_a + \beta_c)} \times \frac{1}{i_{corr}} \quad (2)$$

Since, the i_{corr} values reduced with the increase of percentage loading of PCs in the epoxy resin. Accordingly, the value polarisation resistance (R_p) increased with the increase of polymer composite in epoxy (Table 2). The measured R_p is found to be maximum for specimen PCs3 exhibiting its superior resistance towards diffusive chloride ions [101]. The corrosion protection efficiency (% P.E.) calculated from R_p values are shown in Table 2. % P.E. was determined from the measured R_p {polarisation resistance of epoxy coated mild steel (R_{ps}) and polarisation resistance of epoxy with different wt% loading of PCs coated mild steel (R_{pc})} values by using equation 3.

$$\%P>E> = \frac{R_{pc} - R_{ps}}{R_{pc}} \times 100 \quad (3)$$

The P.E. is observed to be 81.54%, 98.73% and 99.92% for specimens PCs1, PCs2 and PCs4, respectively. Up to 99.95 % P.E. was achieved for sample PCs3 (epoxy coating with 3 wt % loading of polymer composite).

Sample Name (%P.E)	R_p (Ω)	Protection Efficiency
EC	31.8×10^3	-----
PCs1	172.6×10^3	81.5
PCs2	2523.4×10^3	98.7
PCs3	77280×10^3	99.9
PCs4	45310×10^3	99.9

Table 3. Protection efficiency (%P.E.) calculated using polarisation resistance (R_p)

Another parameter that allows the evaluation of barrier nature of a surface coating is the cross linking density. It is reported that higher the cross linking density of the coating, lower is the diffusion of electrolyte through it [48]. The values of glass transition temperature (T_g) shows the extent of cross linking and is directly proportional to the cross linking density. Figure 9 shows the DSC curves of epoxy and epoxy with different wt% loading of polymer composites (PCs). The observed values of T_g are mentioned in Table 3. The T_g for epoxy is measured to be less than the epoxy with polymer composites. It shows the higher cross linking density of epoxy with PCs. Further, the T_g increases gradually with the increase of wt% loading of polymer composite in the epoxy system. This clearly indicates a better cross linking and hence low extent of electrolyte diffusion with the increase wt% of polymer composite. The results are in good agreement with the Tafel extrapolation test results.

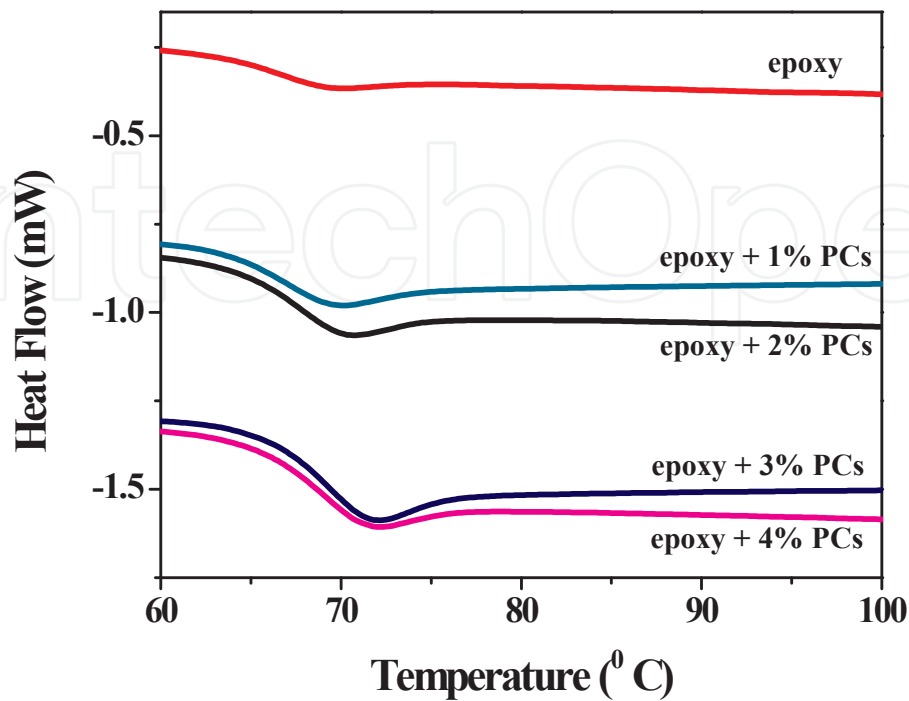


Figure 9. DSC thermograms of epoxy alone and epoxy with different wt% loading of polypyrrole/SiO₂ composites (PCs) recorded after second heating, at a heating rate of 10° C/min in nitrogen atmosphere. (Progress in Organic Coatings DOI: 10.1016/j.porgcoat.2014.04.013).

Loading level of Composite	T _g (° C)
0%	65.2
1.0%	66.6
2.0%	67.3
3.0%	69.2
4.0%	69.8

Table 4. Glass transition temperature (T_g) obtained after second heating.

4.5.2. EIS study

Electrochemical Impedance Spectroscopy (EIS) is a non-destructive electrochemical method used to estimate the performance of the coatings against corrosion. Impedance measurements were carried out at open circuit conditions in 3.5% NaCl solution at room temperature. The impedance graphs obtained for epoxy coated (EC) and epoxy with different wt% loading of polymer composites (PCs1, PCs2, PCs3 and PCs4) coated steel specimens are displayed in Nyquist (Figure. 10) and Bode plots (Figure. 11). The Nyquist plots for epoxy with polymer

composite coated mild steel specimens show much higher impedance value (almost a straight line, Figure. 10c and d) as compared to epoxy coated specimen. However no apparent time constant can be resolved in the plots except for epoxy coating with 2 wt% loading of polymer composite (Figure 10b). So, an attempt to fit the equivalent circuit for the extraction of impedance parameters failed for coated specimens. The Nyquist plot for specimen PCs2 can be differentiated into a high frequency capacitive behaviour followed by low frequency diffusion controlled behaviour of the coating. The high frequency part of the plot represents the property of the coating, whereas, the low frequency part is associated with the Faradiac processes occurring at coating/metal interface through pores and cracks present in the coating [102]. The high frequency capacitive behaviour of the specimen PCs2 demonstrates the corrosion resistance property, while low frequency diffusion behaviour indicated occurrence of diffusion process at the coating/metal interface. Warburg impedance Z_w represents the porosities present in the coating, is expressed in equation 4.

$$Z_w = \sigma \omega^{-1/2} \quad (4)$$

Here, σ is the Warburg coefficient and ω is the angular frequency ($2\pi f$) at which the Warburg diffusion starts. The value of Warburg coefficient (σ) is calculated to be $17.7 \times 10^5 \Omega \text{cm}^{-1}$ (by putting the value of Z_w at frequency 12.1 Hz, where diffusion process starts). Further, the Nyquist plots for epoxy coating with 3 and 4 wt% loading of polymer composite (Figure 10 c and d) show capacitive property similar to an undamaged coating with significantly high impedance in the high frequency region. However, scattering of data points is noticed in the lower frequency region, is basically due to the surface heterogeneities.

The corresponding Bode plots are more informative, as it gives simultaneous measurement of modulus of impedance $|Z|$ with respect to frequency. The Bode plots, as shown in Figure 11 exhibit high frequency region due to the coating capacitance (C_c) and low frequency region due to the charge transfer processes occurring at solution/coating interface [103-105]. The Bode plots of specimens PCs3 and PCs4 show a straight line (slope-1) with high modulus of impedance ($|Z|$) in the high frequency region. This signifies the excellent barrier property of the surface film [106]. However, the slope of the plot becomes -1/2 in the lower frequency region (Figure 11). This is could be due to the adsorbed water on the surface of the coated sample. The value of $|Z|$ in the low frequency region signifies the good barrier property of the surface film [106]. The measured value of $|Z|$ (Table 4) is found to be significantly high ($64940 \times 10^3 \Omega \text{cm}^2$) for the specimen PCs3 (epoxy coating with 3.0 wt% loading of PCs). The magnitude of $|Z|$ at low frequency dropped gradually following the trend from specimens PCs3, PCs4, PCs2, PCs1 to EC (Table 4). The capacitance of the coating (C_c) is an important parameter to evaluate the failure of the coating, as it determines the extent of water uptake [106, 107]. The capacitance of a coating is related to $|Z|$ by equation (4).

$$|Z| = \frac{1}{2\pi f C_c} \quad (5)$$

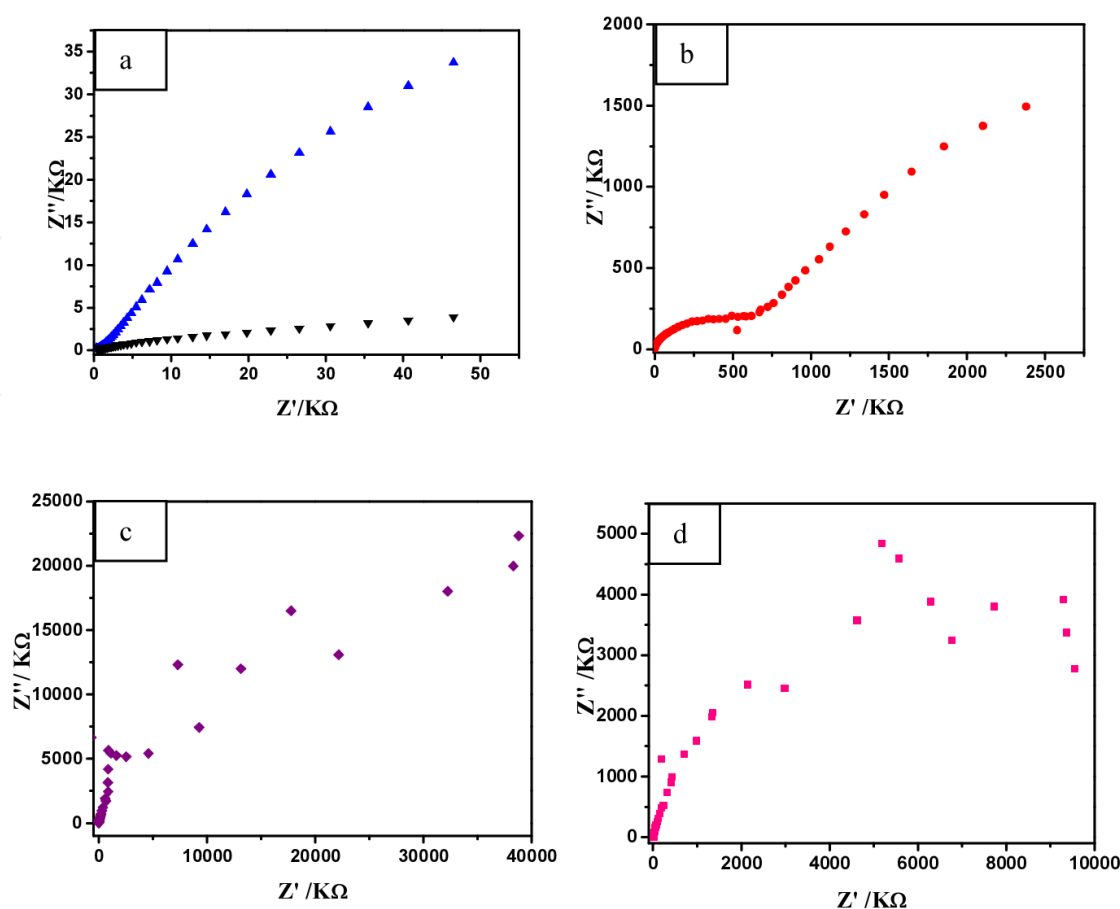


Figure 10. Nyquist plots of epoxy coated (\blacktriangledown) and epoxy with 1.0 wt% (\blacktriangle), 2.0 wt% (\bullet), 3.0 wt% (\blacklozenge) and 4.0 wt% (\blacksquare) loading of polypyrrole/SiO₂ composite (PCs) coated mild steel specimens in 3.5% NaCl solution at room temperature (25±3°C). (Progress in Organic Coatings DOI: 10.1016/j.porgcoat.2014.04.013).

Where, f is the frequency of the applied AC voltage. The values of coating capacitance (C_c) are mentioned in Table 4. The measured C_c is found to be minimum for specimen PCs3 (2.44×10^{-8} F/cm²) exhibiting the undamaged coating formed with 3.0 wt% loading of polymer composite in epoxy. The EIS data clearly shows the superior corrosion resistance property of epoxy coating with 3.0 wt% loading of PCs. The EIS data are in accordance with the Tafel polarisation test results.

From the above electrochemical measurements, it is clear that the polymer composite has made a significant improvement in the corrosion resistance properties of the conventional epoxy coatings in 3.5% NaCl solution. However, it is necessary to evaluate the corrosion resistance of the coating for relatively longer period of exposure to corrosive electrolyte. Since, epoxy with 3 wt% loading of polymer composite coated steel specimen (PCs3) has shown the superior corrosion resistance amongst the coated specimens, therefore, it has been considered for periodic impedance measurement. Figure 12 shows the variation of modulus of impedance ($|Z|$) and coating capacitance (C_c) with the immersion time. The magnitude of impedance reduced significantly for the first 10 days of immersion. This is basically due to the weakening

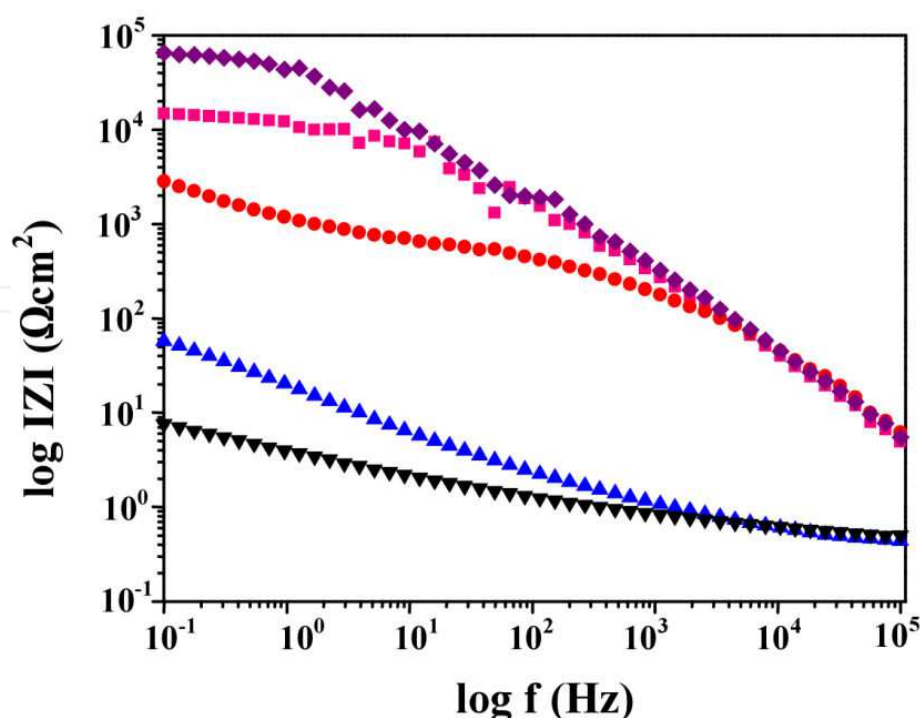


Figure 11. Bode plots of epoxy coated (▼) and epoxy with 1.0 wt% (▲), 2.0 wt% (●), 3.0 wt% (◆) and 4.0 wt% (■) loading of polypyrrole/SiO₂ composite (PCs) coated mild steel specimens in 3.5% NaCl solution at room temperature (25 ± 3°C). (Progress in Organic Coatings DOI: 10.1016/j.porgcoat.2014.04.013).

Sample Name	Loading level of composite	Z (KΩ cm ²)	C _c (F/cm ²)
EC	0 %	7.5	2.1 x 10 ⁻⁴
PCs1	1.0 wt%	57.4	2.7 x 10 ⁻⁵
PCs2	2.0 wt%	2810	5.6 x 10 ⁻⁷
PCs3	3.0 wt%	64940	2.4 x 10 ⁻⁸
PCs4	4.0 wt%	14750	1.0 x 10 ⁻⁷

Table 5. Different electrochemical parameters extracted by EIS measurements for epoxy and epoxy with different wt % loading of polymer composite in 3.5% NaCl solution.

of the barrier property of the surface film due to diffusive chloride ions. Accordingly, an increase in coating capacitance (C_c) is noticed for this period. The increase in the value of coating capacitance is due to the electrolyte uptake with the passage of immersion time [108, 109]. The high dielectric constant of water ($\epsilon=80$) increases the dielectric constant of the organic coatings when exposed to it leading to increase of coating capacitance [110]. The above observations reveal the weakening of the barrier property of the coating with immersion time. However, the coating capacitance becomes almost constant after 15 days of immersion. This could be due to the clogging of the pores of the coatings by the corrosion products. Interestingly, the measured $|Z|$ for specimen PCs3 after 20 days of immersion (16.6 KΩ cm²) is still

observed to be higher than the freshly immersed epoxy coated specimen ($7.5 \text{ K}\Omega \text{ cm}^2$). Similarly, the C_c for specimen PCs3 after 20 days of immersion ($9.4 \times 10^{-5} \text{ F/cm}^2$) is lower than the freshly immersed epoxy coated specimen ($2.1 \times 10^{-4} \text{ F/cm}^2$). This clearly shows the superior barrier property shown by epoxy coatings with polymer composite.

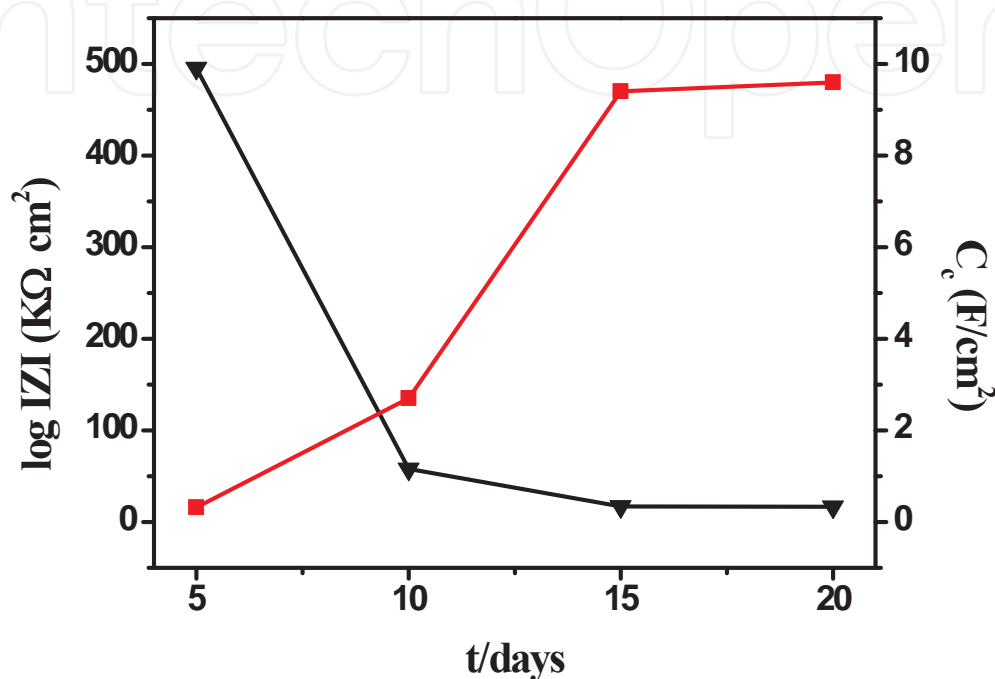


Figure 12. Variation of magnitude of impedance ($|Z|$) and coating capacitance (C_c) with time for epoxy with 3 wt% loading of polymer composite coated steel specimen exposed to 3.5% NaCl solution. (Progress in Organic Coatings DOI: 10.1016/j.porgcoat.2014.04.013).

4.5.3. Salt spray test

Figure 13 shows the photographs of epoxy coated (EC) and epoxy with different wt% loading of polymer composites (PCs1, PCs2, PCs3 and PCs4) coated steel panels after exposure to salt spray fog for 65 days. Figure 13a clearly shows the occurrence of severe rusting throughout the scribe mark for epoxy coated steel panel. The under film blisters were also noticed visually. The presence of rust and blisters indicates loss of adherence of the epoxy coating during prolong exposure to salt fog. The presence of polymer composites in epoxy improves the corrosion resistance properties of the steel, which can be noticed from the photographs (Figure 13b-e). The epoxy with 1.0 and 2.0 wt% loading of PCs coated steel panels exhibit less extended corrosion along the scribe mark (Figure 13b and c). Further, the extended corroded area along the scribe mark almost disappeared for steel panels coated with epoxy with 3.0 and 4.0 wt% loading of PCs (Figure 13d and e). The results clearly show that the epoxy powder coating formulations incorporating polypyrrole/ SiO_2 composites are very effective in preventing

corrosion and blistering near the scribe mark when exposed to environmental conditions of high humidity and high salt content. The remarkably high corrosion protection of epoxy coatings with polymer composites as compared to epoxy coating alone is due to the dual protection mechanism by the synthesized composite in the coating system. Polypyrrole forms a passive layer and simultaneously act as a physical barrier between metal and electrolyte. On the other hand, SiO_2 particles as filler in polypyrrole matrix provide mechanical integrity and reduce the degradation of polymer composite coating under corrosive conditions.

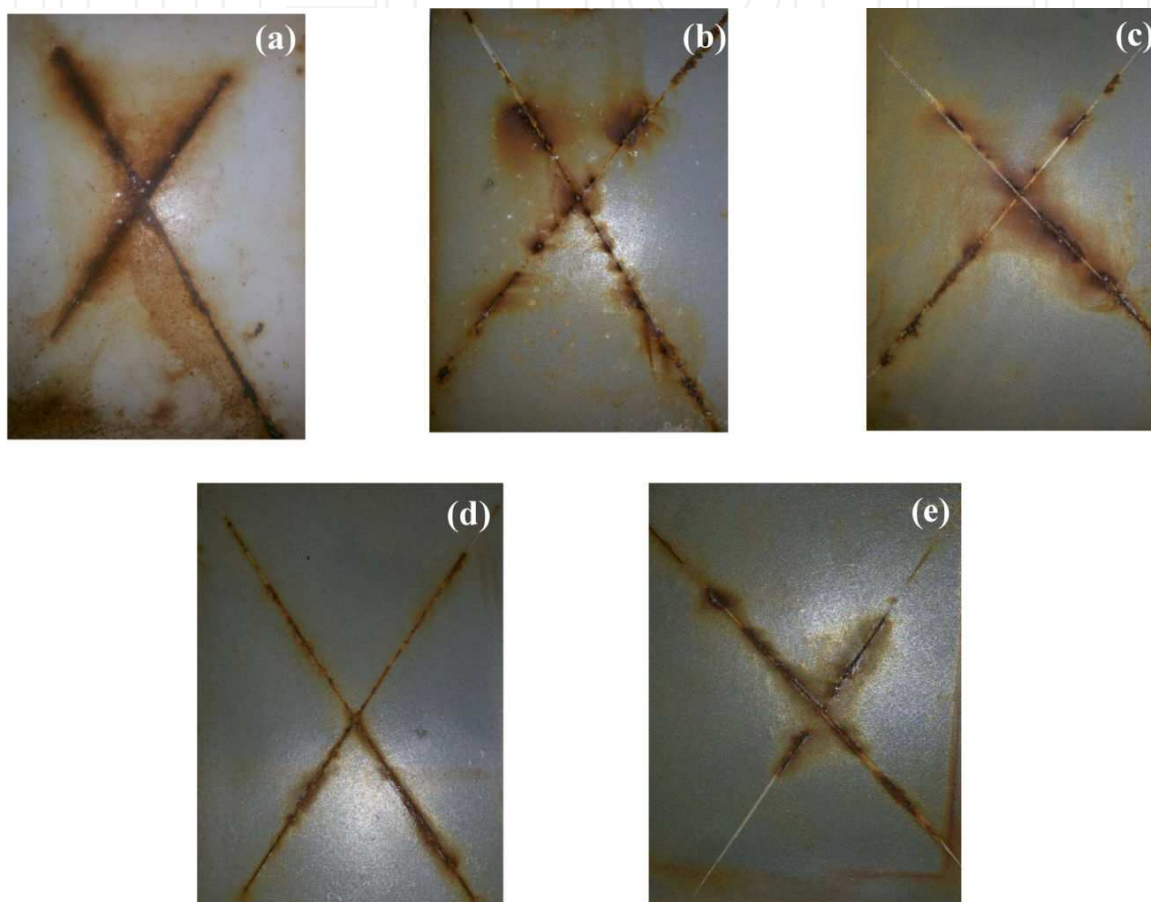


Figure 13. Photographs of (a) epoxy coated and epoxy with (b) 1.0 wt%, (c) 2.0 wt%, (d) 3.0 wt% and (e) 4.0 wt% loading of polypyrrole/ SiO_2 composite (PCs) coated mild steel specimens exposed to salt spray fog after 65 days. (Progress in Organic Coatings DOI: 10.1016/j.porgcoat.2014.04.013).

5. Anti corrosive properties of chitosan/polymer composite in 3.5% NaCl solution

5.1. Synthesis of chitosan/polypyrrole/ SiO_2 composite (CsPC)

Chitosan with a degree of deacetylation 90% was a fine pale yellow powder (100 mesh) ground from shrimp shell was used for the synthesis of the composite. The synthesis of mono dispersed

uniform-sized SiO_2 particles were carried out by hydrolysis of tetra-ethyl orthosilicate (TEOS) in ethanol using ammonia as a catalyst as mentioned in section 3.1. Chitosan/polymer composites (CsPC) were synthesized by chemical oxidative polymerization of pyrrole monomer in presence of 1wt% chitosan solution (in 1% acetic acid) [111]. For this, a mixture of 1 gm chitosan (Cs), 1 gm acetic acid and 98 gms of deionized water was stirred till a clear pale solution (pH ~ 3) of chitosan acetate appears [112]. The synthesized silica particles were dispersed in suspension of sodium lauryl sulphate (SLS) in distilled water. The suspension was added to chitosan solution and was allowed to stir for 20 minutes. It is reported that chitosan interacts with anionic surfactants by electrostatic attraction to form soluble complexes [113, 114]. Thereafter, pyrrole was introduced in it, followed by drop by drop addition of freshly prepared FeCl_3 to initiate the polymerization of pyrrole. The molar ratio of FeCl_3 : pyrrole : SLS was taken to be 1:1:0.5. The resultant composite was filtered and washed with water and ethanol to remove oligomers and oxidant. Thereafter, it was dried in a vacuum oven at 60°C . The schematic of the synthesis of chitosan/polymer composite is shown in Figure 14.

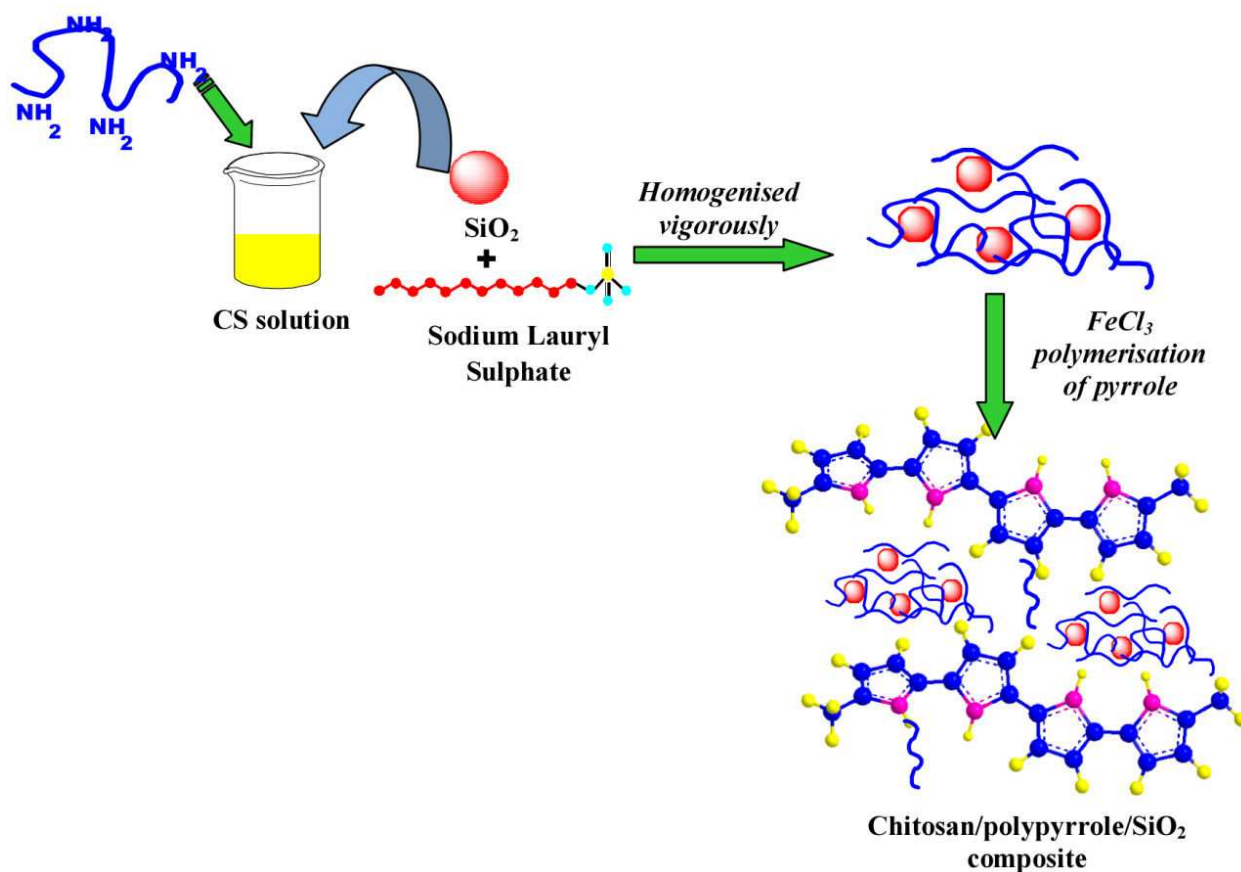


Figure 14. Schematic of the synthesis of chitosan/polypyrrole/ SiO_2 composites. (Communicated to Progress in Organic Coatings, Ref. 110, Elsevier)

5.2. Powder coating on mild steel surface

Mild steel specimens were polished metallographically, prior to the development of coating. The powder coating formulations were prepared by blending composites in epoxy resin. A homogenous mixture of well dispersed composites in epoxy was obtained after ball milling treatment. The coatings were applied on mild steel specimens using an electrostatic spray gun held at 67.4 KV potential with respect to the substrate (grounded). The powder coated mild steel specimens were cured at 140°C for 30 minutes. The adhesion of the coating was tested by tape test as per ASTM D3359-02 and found to pass the test.

6. Characterization of chitosan/polymer composites

6.1. FTIR spectra

The FTIR spectrum of chitosan, as shown in Figure 15 exhibits an intense broad band in the spectral range of 3200-3650 cm^{-1} . It is attributed to the axial stretching of O-H and N-H bonds. A small band near 2870 cm^{-1} is due to the C-H stretching vibration. A peak of considerable intensity at 1650 cm^{-1} is assigned to amide I vibration and peaks at 1426 and 1382 cm^{-1} is the result of coupling of C-N axial stretching and N-H angular deformation. The peaks at 1155, 1074 and 1024 cm^{-1} corresponds to the stretching vibration of C-O-C linkage in the glucosamine rings. The FTIR spectrum of chitosan-polypyrrole composite (CP) exhibits a broad band at 3421 cm^{-1} showing the N-H stretching of pyrrole and O-H stretching of chitosan. The characteristic peaks of polypyrrole at 1546 cm^{-1} (C=C benzoic form), 1458 cm^{-1} (C-N stretching) was observed with considerable intensity [115-117]. The peak at 1172 cm^{-1} (S-O stretching) and 1035 cm^{-1} (S-C stretching) confirm the formation of chitosan/polypyrrole composite doped with SLS. It is important to note that the reported peak for S-O stretching for polypyrrole occurs at 1168 cm^{-1} , which has been shifted to 1172 cm^{-1} for the composite. It clearly shows interaction of chitosan and polypyrrole with SLS. The corresponding peak for amide vibration at 1650 cm^{-1} of chitosan was not observed for the composite. This shows the presence of mainly protonated amino groups as a result of dissolution of chitosan in acetic acid. The other peaks at 902, 768 and 670 cm^{-1} are due to the C-H out of plane deformation vibration of the ring. An additional peak of considerable intensity appears at 1108 cm^{-1} , solely due to the presence of SiO_2 in chitosan/polypyrrole/ SiO_2 composite (CsPC). However, this peak is slightly shifted, as the peak for Si-O-Si stretching in SiO_2 occurs at 1080 cm^{-1} . The shifting of the peak could be due to the adsorption of chitosan/polypyrrole on the surface of silica particles. It is reported that chitosan provides the formation of active sites for grafting of polypyrrole chains on silica particles and acts as a stabilizer of silica-polypyrrole particles [118]. The FTIR results exhibit strong interaction between chitosan, polypyrrole and silica in the composite.

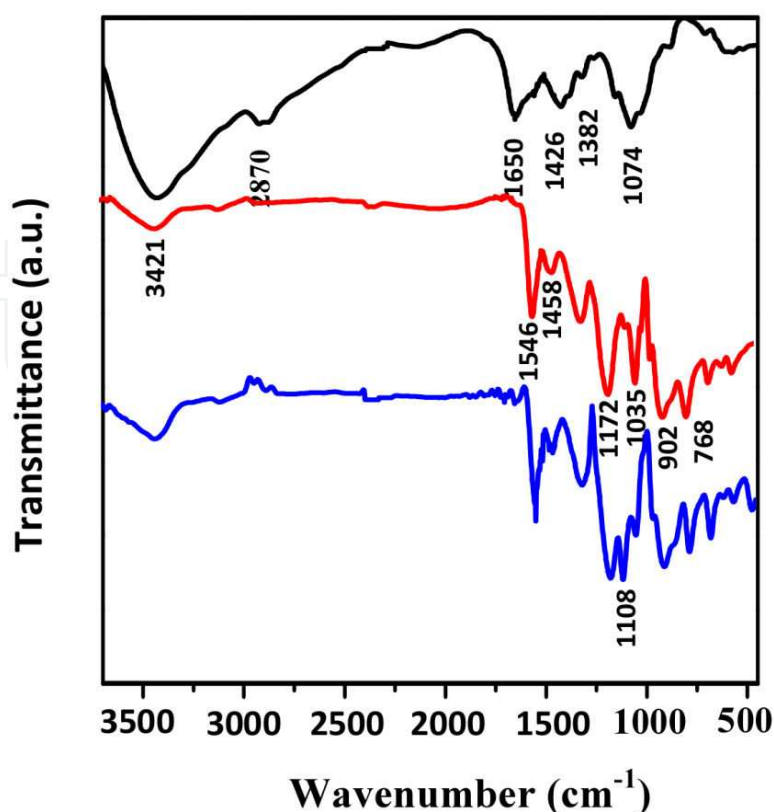


Figure 15. FTIR spectra of chitosan (—), chitosan/polypyrrole (—) and chitosan/polypyrrole/SiO₂ (—) composite. (Communicated to Progress in Organic Coatings, Ref. 110, Elsevier)

6.2. XRD diffraction

The XRD diffraction patterns of chitosan (a) and chitosan/polypyrrole/SiO₂ composite (CsPC) are presented in Figure 16. The presence of a scattering peak at 2θ value 19.88° corresponding to (020) plane is basically due to the semi crystalline nature of chitosan [119, 120]. The diffractogram of CsPC showed a broad scattering peak at approximately 26° – 27° , which indicates a highly amorphous structure of the composite. This shows the interaction between chitosan and polypyrrole. The absence of corresponding peaks of silica is due to the uniform covering of polypyrrole chains on the silica particles [118].

6.3. Thermogravimetric analysis of composites

TGA curves for chitosan, chitosan/polypyrrole (CP) and chitosan/polypyrrole/SiO₂ (CsPC) composites are presented in Figure 17. The curves were recorded by heating the samples from 25° to 800° C under constant heating rate of $15^\circ\text{C}/\text{min}$ under nitrogen atmosphere (60 ml/min). The first stage of all the three curves shows 10% weight loss between 25° to 145° C. The weight loss is attributed to the loss of moisture and other volatile compounds. The second weight loss of 34 % for chitosan occurs at 240° C, is mainly due to thermal decomposition of chitosan [121, 122]. The second weight loss due to thermal decomposition of polymer composites is delayed to 260° and 265° C for CP and CsPC, respectively. Additionally, the chitosan and CP showed a

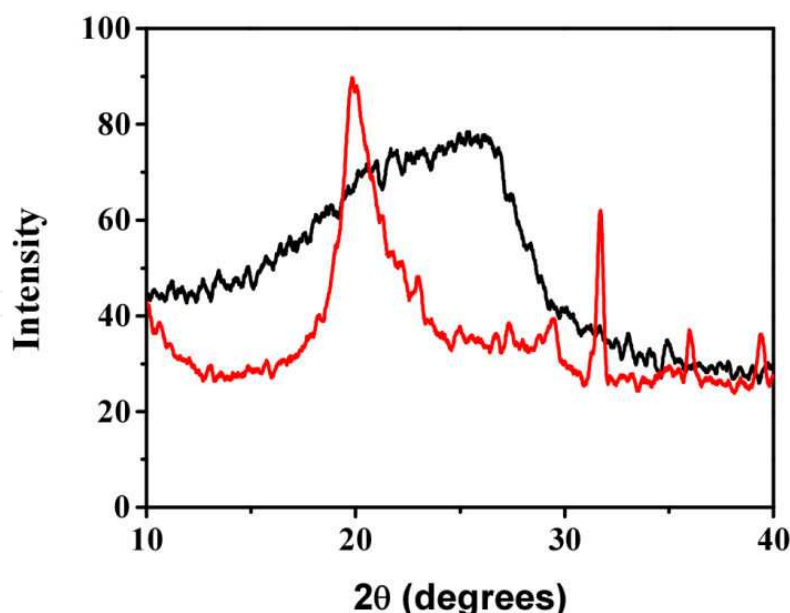


Figure 16. XRD graphs of (a) chitosan and (b) chitosan/polypyrrole/SiO₂ composite. (Communicated to Progress in Organic Coatings, Ref. 110, Elsevier)

weight loss of 61% and 54%, respectively at 800° C. The comparatively less weight loss of chitosan/polypyrrole composite (CP) as compared to chitosan shows the better thermal stability of composite. The incorporation of SiO₂ in the polymer matrix further improves the thermal stability of the composite as the weight loss at 800° C was only 49%. The increase in thermal stability of CsPC can be attributed to the better thermal stability of silica particles and to the interactions between silica and chitosan/polypyrrole.

6.4. SEM/TEM images of chitosan/polymer composites

Figure 18 (a-c) depict the FE-SEM and TEM images of composites. The FE-SEM image of the chitosan/polypyrrole/SiO₂ composite (CsPC) reveals a clustered structure composed of spherical nano particles (diameters ~ 40-50 nm) of polypyrrole and chitosan (Figure 18 a). The presence of SiO₂ particles embedded in chitosan/polypyrrole matrix can easily be noticed in the micrograph. The TEM image of CsPC (Figure 18 b) exhibits the presence of distinct spherical nano particles of chitosan and polypyrrole arranged in a regular pattern. It is reported that the polymerisation of pyrrole in absence of chitosan, forms polypyrrole particles having diameters 100-150 nm with aggregated cauliflower morphology [69]. On the other hand, the in situ chemical polymerisation of pyrrole in presence of chitosan causes the formation of much smaller polypyrrole nano spheres (40-60 nm). Here, chitosan acts as a steric stabiliser and hinders the formation of large size polypyrrole particles [67]. The TEM micrograph of polypyrrole/SiO₂ composite (PS) (Figure 18c) shows the presence of large size polypyrrole particles with diffused morphology. The EDAX spectrum of CsPC confirms the presence of carbon, nitrogen, sulphur, oxygen and silicon in the composite. The microstructural features of the composites are in good agreement with the FTIR results showing strong interaction between polypyrrole and chitosan.

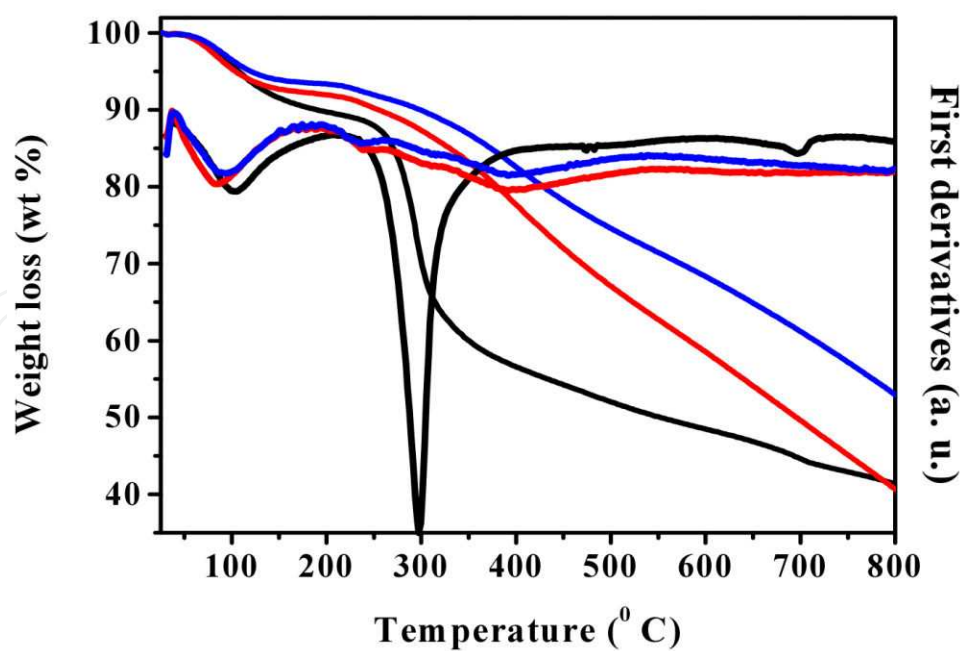


Figure 17. TGA curves of chitosan (—), chitosan/polypyrrole (—) and chitosan/polypyrrole/SiO₂ (—) composite. (Communicated to Progress in Organic Coatings, Ref. 110, Elsevier)

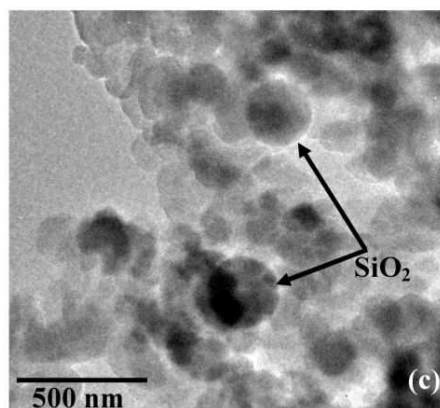
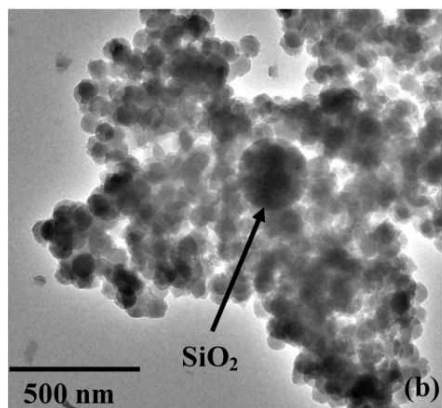
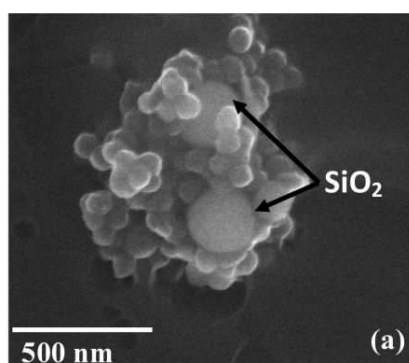


Figure 18. (a) FESEM micrograph of chitosan/polypyrrole/SiO₂ composite. TEM micrographs of (b) Chitosan/polypyrrole/SiO₂ and (c) polypyrrole/SiO₂ composites. (Communicated to Progress in Organic Coatings, Ref. 110, Elsevier)

6.5. Corrosion studies of chitosan/polymer composites in 3.5% NaCl solution

6.5.1. Tafel polarisation

Figure 19 shows the Tafel polarisation curves for epoxy coated (EC) and epoxy with different wt% loadings of chitosan/polymer composite coated steel specimens (CsPC1 for 1.0%, CsPC2 for 2.0% and CsPC3 for 3.0%) exposed to 3.5% NaCl solution. For comparative studies Tafel plots are drawn for polypyrrole/SiO₂ composite with 4 wt% loading in epoxy, PCs4 (without chitosan) and chitosan/polypyrrole composite (CP) (without SiO₂) coated steel specimens. Different electrochemical parameters, such as corrosion potential (E_{corr}) and corrosion current density (i_{corr}) are derived from curve fitting method and are summarized in Table 5.

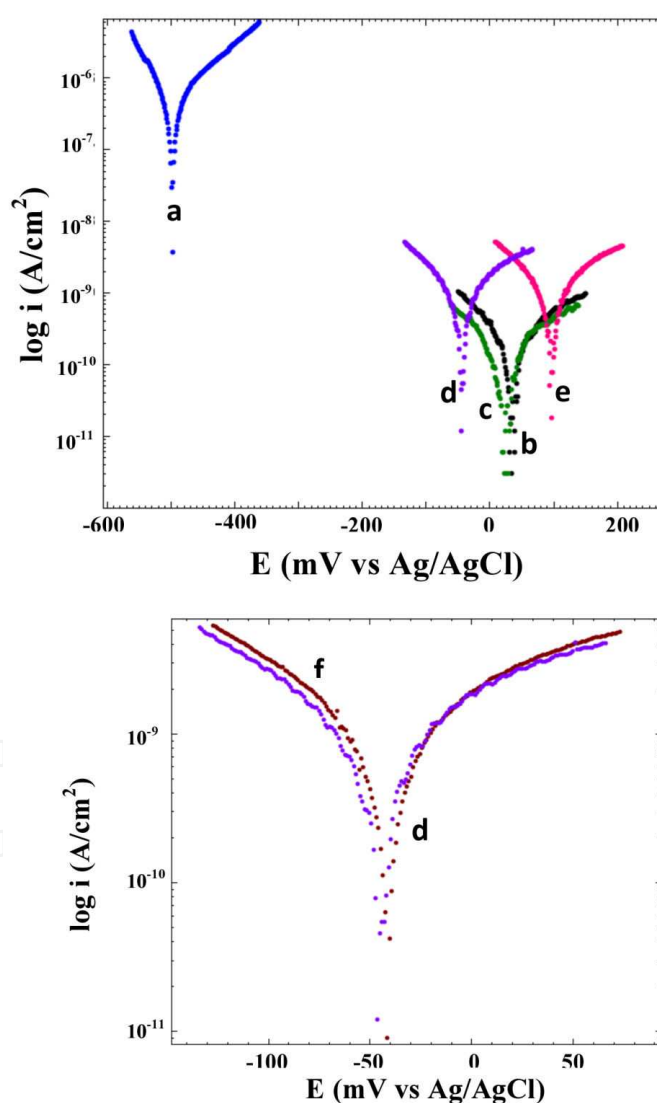


Figure 19. (a) Tafel plots of (a) epoxy coated and epoxy with (b) 1.0 wt%, (c) 2.0 wt%, (d) 3.0 wt% chitosan/polypyrrole/SiO₂ composite, (e) polypyrrole/SiO₂, (f) chitosan/polypyrrole composite coated mild steel specimens in 3.5% NaCl solution at room temperature (25±3°C). (Communicated to Progress in Organic Coatings, Ref. 100, Elsevier)

The E_{corr} for epoxy coated mild steel is observed to be -582.09 mV. One can notice a remarkable shift of E_{corr} in the noble direction for all the composite coated steel specimens exhibiting the presence of corrosion resistant passive layer on the metal surface. The E_{corr} of specimen PCs4 occurs at 95.43 mV. It is important to mention that the polypyrrole/SiO₂ composite coating (PCs4) that was taken for the comparative studies is developed by 4.0 wt % loading in epoxy powder formulation. Accordingly, the i_{corr} value of PCs4 is observed to be three orders of magnitude less than the epoxy coated steel, showing its superior corrosion resistance property. On the other hand, the chitosan/polypyrrole/SiO₂ composite coated steel specimens, CsPC1 and CsPC2 show the E_{corr} values 36.46 mV and 20.75 mV, respectively, (Table 5) which was slightly less than the E_{corr} observed for specimen PCs4. However, the corrosion current density (i_{corr}) values of CsPC1 and CsPC2 were found to be almost 7.73 and 16 times respectively less as compared to the specimen PCs4. The significantly less i_{corr} values for the chitosan/polypyrrole/SiO₂ composite coated specimens clearly exhibit the efficient role of chitosan in enhancing the corrosion protection tendency of the composite. It is be due to the synergistic effect of the chitosan and polypyrrole that resulted in the formation of coatings, which is less susceptible to moisture and prevent the penetration of corrosive ions. Further, the i_{corr} value increased slightly for specimen CsPC3 as compared to CsPC1 and CsPC2. This reveals the deterioration of corrosion protection tendency of the composite coating with further increase of the percentage loading in the epoxy. The 2.0 wt% loading of CsPC in epoxy could be the best possible combination of coating formulation. The role of SiO₂ particles cannot be ignored in the composite system, as the E_{corr} and i_{corr} values of specimen CP is found to be almost equal to the specimen CsPC3 (the chitosan/polymer composite coated specimen with least corrosion resistance). The better thermal stability of chitosan/polypyrrole/SiO₂ composite is discussed in TGA analysis. The remarkably high corrosion resistance of chitosan/polypyrrole/SiO₂ composite coatings could be due to the combined effect of chitosan and polypyrrole as corrosion inhibitors. The polarisation resistance (R_p) values are related to corrosion current density (i_{corr}), which is directly proportional to corrosion rate through Stern-Geary equation as mentioned in equation (2) are also shown in Table 5. The maximum R_p value measured for sample CsPC2, further confirms the superior corrosion resistance property of the epoxy with 2 wt% loading of chitosan/polypyrrole/SiO₂ composite. The maximum of 99.97% corrosion protection efficiency (P.E.) is achieved for specimen CsPC2. So, chitosan/polypyrrole/SiO₂ composite coating with 2.0 wt% loading in epoxy powder formulation exhibits superior corrosion resistance among all test specimens in 3.5% NaCl solution.

Figure 20 shows the DSC thermograms of epoxy and epoxy with chitosan/polypyrrole/SiO₂ (CsPC2), chitosan/polypyrrole (CP) composite. In order to evaluate the role of chitosan in the composite, DSC thermograms of epoxy with polypyrrole/SiO₂ composites (PCs4) are also shown here. The glass transition temperature (T_g) is related to cross linking density [85], that relates to the barrier nature of the surface film. The observed T_g is found to increase with the incorporation of polymer composite in the epoxy resin. The T_g for epoxy with chitosan/polypyrrole/SiO₂ composite (75.1°C) is found to be almost 10°C more than the epoxy resin, showing the higher cross linking density with superior barrier property of the chitosan/polymer composite. On the other hand, the T_g for epoxy with polypyrrole/SiO₂ composite

Sample Name	Loading level of polymer	E_{corr} (mV)	i_{corr} (A/cm ²)	R_p (K Ω)	Protection Efficiency (% P.E.)
EC	-----	-582.49	8.45×10^{-7}	31.87	----
CsPC1	1.0 wt%	36.46	0.50×10^{-9}	105580	99.96
CsPC2	2.0 wt%	20.75	0.24×10^{-9}	156200	99.97
CsPC3	3.0 wt%	-46.68	3.79×10^{-9}	22632	99.85
PCs4	4.0 wt%	83.522	1.51×10^{-9}	45310	99.92
CP	1.0 wt%	-41.62	3.27×10^{-9}	20580	99.84

Table 6. Different electrochemical parameters obtained by Tafel extrapolation in 3.5% NaCl solution.

occurs 6°C less than the epoxy with chitosan/polypyrrole/SiO₂ composite. The excellent film forming tendency of chitosan and the synergistic interaction of chitosan and polypyrrole are the reasons for the occurrence of higher cross linking density of chitosan/polypyrrole/SiO₂. It is reported that higher the cross linking density of the coating, lower is the diffusion of electrolyte through it [85]. Therefore, epoxy with chitosan/polypyrrole/SiO₂ composite has the superior barrier property. The results are in accordance with the Tafel extrapolation test results.

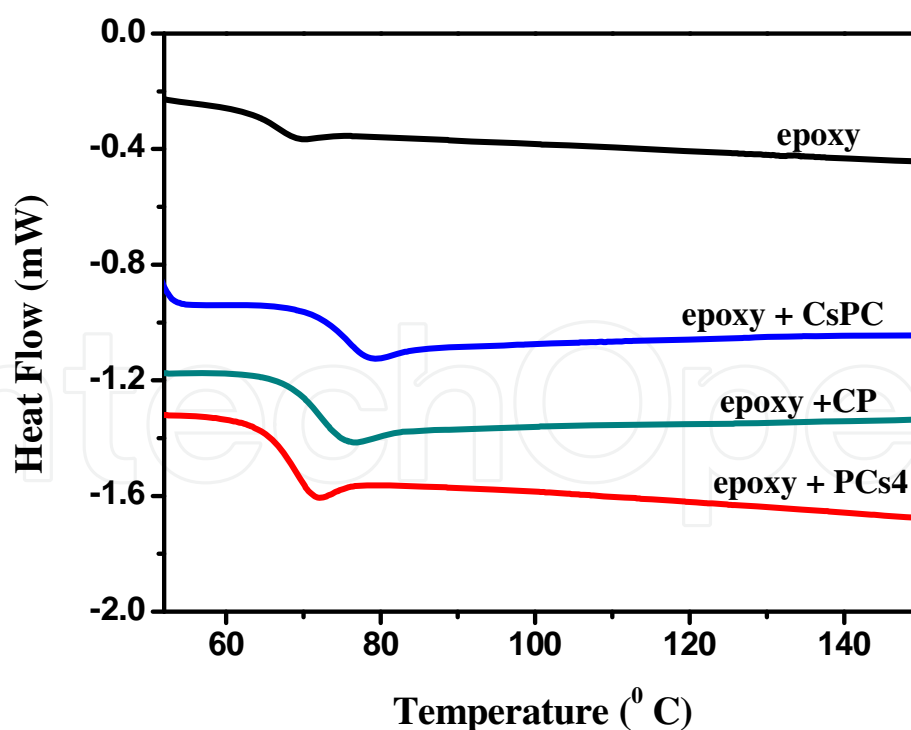


Figure 20. DSC thermograms of epoxy and epoxy with 2% loading of chitosan/polypyrrole/SiO₂ (CsPC), chitosan/polypyrrole composites (CP) and polypyrrole/SiO₂ (PCs4) composite recorded after second heating, at a heating rate of 10° C/min in nitrogen atmosphere. (Communicated to Progress in Organic Coatings, Ref. 110, Elsevier)

Sample name	T_g (° C)
epoxy	65.2
epoxy+CsPC	75.1
epoxy+CP	71.3
epoxy + PCs4	69.2

Table 7. Glass transition temperature (T_g) obtained after second heating.

6.5.2. Electrochemical impedance spectroscopy (EIS)

Impedance measurements were carried out in terms of Bode plots at open circuit conditions in 3.5% NaCl solution at room temperature ($25 \pm 3^\circ \text{C}$). The Bode plots obtained for epoxy coated (EC), chitosan/polypyrrole/SiO₂ composite coated with different wt% loading in epoxy (CsPC1, CsPC2 and CsPC3), chitosan/polypyrrole composite (CP) coated and polypyrrole/SiO₂ composite (PS) coated steel specimens are displayed in Figure 21. Bode plot is informative as it gives simultaneous measurement of modulus of impedance $|Z|$ with respect to frequency. As shown in Figure 21, a high magnitude of impedance ($|Z|$) with a slope of -1 at frequency ~ 10 Hz, for the composite coated steel specimens signify an excellent barrier property of the surface film and correspond to the less corrosive ions being in contact with the metal surface [123]. The respective region for the epoxy coated steel specimen shows a significantly less $|Z|$ (Table 7) revealing its weak barrier property against corrosive ions. Further, the Bode plots show a resistive plateau (horizontal line) in the low frequency region ($< 1\text{Hz}$). The total impedance ($|Z|$) in this region is mainly due to the impedance of the coating defects and can be considered as a measure of coating protectiveness [81, 124]. The magnitude of total impedance for coated specimens, CsPC1 and CsPC2 in this region is found to be four orders of magnitude higher as compared to the epoxy coated steel specimen (Table 7). Although, the $|Z|$ values for specimen CP and PCs4 is almost three orders of magnitude higher as compared to epoxy coated steel (EC). But, $|Z|$ values occur an order of magnitude less than the specimens CsPC1 and CsPC2. A much high magnitude of impedance for chitosan/polypyrrole/SiO₂ composite coated specimens shows the presence of surface film with superior corrosion resistance. However, the low value of impedance for epoxy coated steel is associated with the high defectiveness of the coating. Further, the capacitance of the coating (C_c) is an important parameter to evaluate the failure of the coating as it determines the extent of water uptake [106]. The capacitance of a coating is related to the magnitude of the impedance ($|Z|$) by the equation (3) is given in Table 7. The value of C_c is found to be least for specimen CsPC2 exhibiting the undamaged coating formed with 2.0 wt% loading of chitosan/polypyrrole/SiO₂ composite in epoxy coating formulation. As expected, the highest value of C_c for epoxy coated specimens (EC) shows its greater electrolyte uptake tendency. The observed results are in accordance with the Tafel polarisation results.

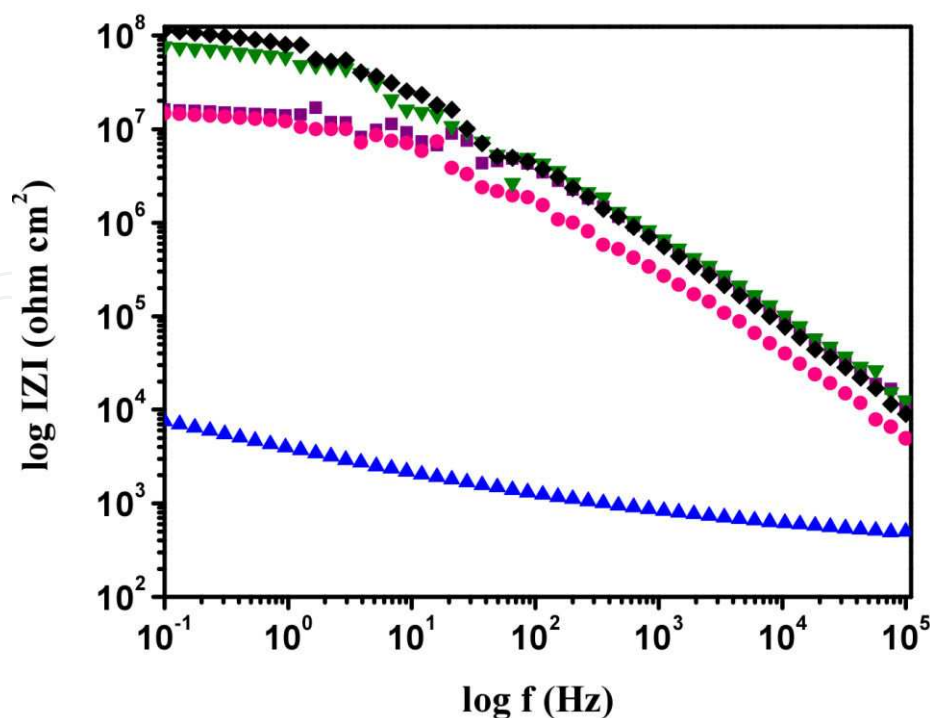


Figure 21. Bode plots of epoxy coated (\blacktriangle) and epoxy with 1.0 wt% (\blacktriangledown), 2.0 wt% (\blacklozenge), 3.0 wt% (\blacksquare) and polypyrrole/ SiO_2 composite ($*$) coated mild steel specimens in 3.5% NaCl solution at room temperature ($25\pm 3^\circ\text{C}$). (Communicated to Progress in Organic Coatings, Ref. 110, Elsevier)

Sample Name	Loading level of polymer	$ Z $ ($\text{K}\Omega \text{ cm}^2$)	C_c (F/cm^2)
EC	0 %	7.55	2.1×10^{-4}
CsPC1	1.0 wt%	76669	2.0×10^{-8}
CsPC2	2.0 wt%	104200	1.5×10^{-8}
CsPC3	3.0 wt%	16220	9.9×10^{-8}
PCs4	4.0 wt%	14750	1.0×10^{-7}
CP	1.0 wt%	16281	2.7×10^{-7}

Table 8. Different electrochemical parameters extracted by EIS measurements in 3.5% NaCl solution.

6.6. Salt spray tests

Salt spray tests results are displayed in Figure 22. Figure shows the photographs of epoxy coated (a) and epoxy with different wt% loading of polymer composites, CsPC1 (b), CsPC2 (c), CsPC3 (d), CP (e) and PCs4 (f) coated steel panels after exposure to salt spray fog for 65 days. Figure 22a clearly shows rusting throughout the scribe mark for epoxy coated steel panel. The presence of rust and blisters indicates the loss of adherence of the epoxy coating during prolong exposure to salt fog. The incorporation of chitosan/polypyrrole/ SiO_2 composites (CsPC) in epoxy improve the corrosion resistance properties of the steel that can be noticed from the photographs (Figure 22b-d). The epoxy with 1.0 and 2.0 wt% loading of CsPC coated

steel panels exhibit a less corrosion along the scribe mark (Figure 22b and c). However, the corrosion near scribe mark is visible for steel panels coated with epoxy with 3.0 % loading of CsPC (Figure 22d). The results clearly show that the epoxy powder coating formulations incorporating chitosan/polypyrrole/SiO₂ composites are very effective in preventing corrosion and blistering near the scribe mark when exposed to environmental conditions of high humidity and high salt content. Extended corrosion is noticed for steel panel coated with epoxy with chitosan/polypyrrole composite exhibiting the less protective nature of surface film (Figure 22e). The appreciable high E_{corr} noticed for steel coated with epoxy with 4.0 % loading of polypyrrole/SiO₂ composite (PS) is supported by less extended corroded area along the scribe mark (Figure 22f). Amongst all, the remarkably high corrosion protection of chitosan/polypyrrole/SiO₂ composite coatings is due to the protection offered by chitosan and polypyrrole present in the coating system. The film forming tendency of chitosan and passive layer formation of polypyrrole acts as a physical barrier between metal and electrolyte. On the other hand, SiO₂ particles as filler in chitosan/polypyrrole matrix provide mechanical integrity and reduce the degradation of polymer composite coating under corrosive conditions.

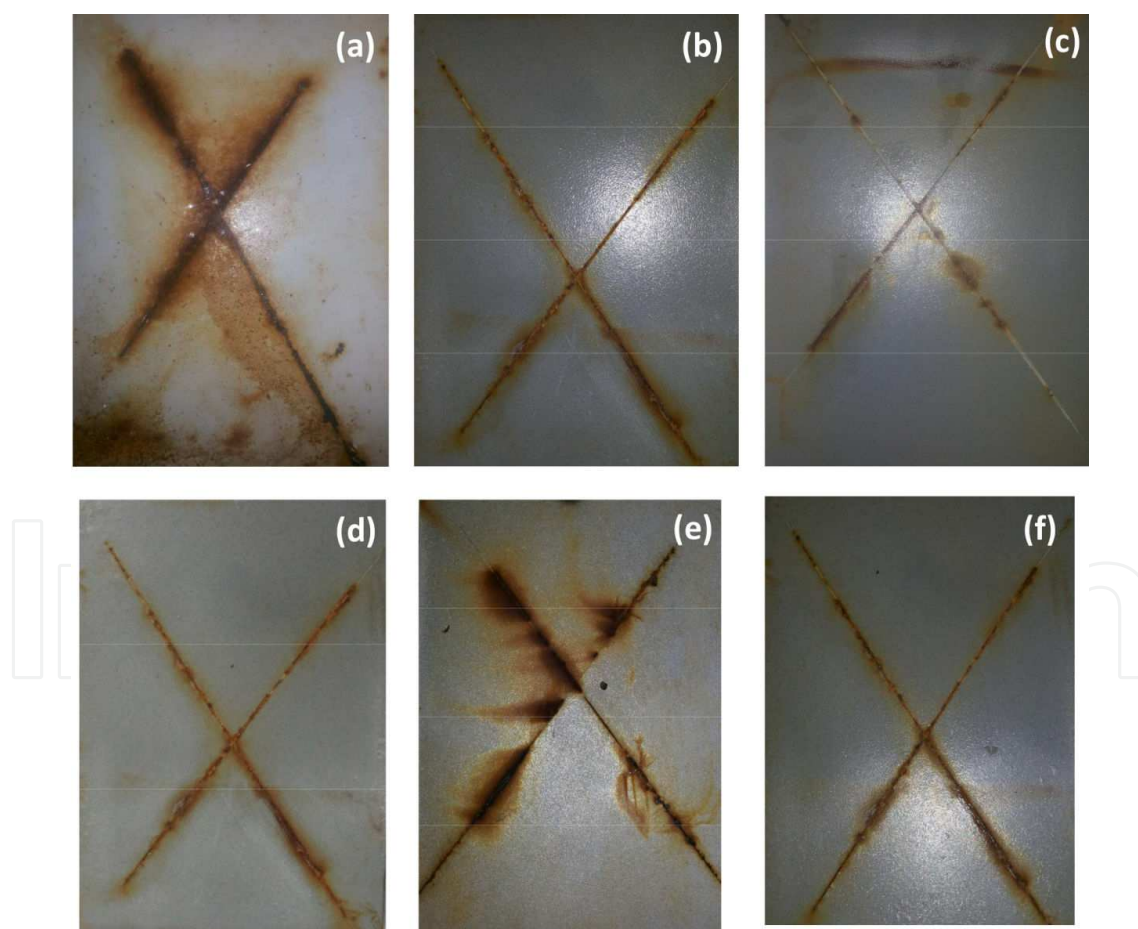


Figure 22. Photographs of (a) epoxy coated and epoxy with (b) 1.0 wt%, (c) 2.0 wt%, (d) 3.0 wt% loading of chitosan/polypyrrole/SiO₂, (e) chitosan/polypyrrole and (f) polypyrrole/SiO₂ composite coated mild steel specimens exposed to salt spray fog after 65 days. (Communicated to Progress in Organic Coatings, Ref. 110, Elsevier)

7. Conclusions

In present study, corrosion resistance of mild steel specimens coated with conventional epoxy coating and epoxy with different wt% loading of polypyrrole/SiO₂ and chitosan/polypyrrole/SiO₂ composites were evaluated by means of Tafel extrapolation, electrochemical impedance spectroscopy and salt spray tests in highly corrosive conditions. The electrochemical measurements and salt spray tests suggest that mild steel specimens coated with epoxy coatings with polypyrrole/SiO₂ composites (PCs) makes a remarkable improvement in the corrosion resistance properties as compared to conventional epoxy coatings. The corrosion protection efficiency (% P.E.) increases with the increase of percentage loading of PCs in epoxy resin. A maximum P.E. of 99.95 % is achieved for coating with 3.0 wt% loading of PCs, thereafter, it reduced slightly for coating with 4.0 wt% loading of PCs. The incorporation of chitosan (biopolymer) in the polypyrrole/SiO₂ system further improves the corrosion resistance of the steel specimens. Corrosion protection efficiency (%P.E.) of 99.97 is achieved for the 2 wt% loading of chitosan/polypyrrole/SiO₂ composites in the epoxy resin. The salt spray test results show a highly extended corroded area along the scribe mark for the epoxy coated steel panel. Whereas, presence of polymer composites (polypyrrole/SiO₂ and chitosan/polypyrrole/SiO₂) in the epoxy system appears to inhibit the extended corrosion as almost no corrosion or blistering is noticed for the mild steel specimen coated with epoxy with polymer composites. The above results reveal that the synthesized polymer composites interacts with the epoxy resin to form well adherent, high quality, superior anti corrosive coatings on mild steel surface using powder coating technique.

Acknowledgements

Authors thank the Director, National Physical Laboratory, CSIR, New Delhi for providing the laboratory facilities for conducting experiments and characterizations. Their thanks are extended to Mr. Brij Bisht for salt spray test results. One of the authors Gazala Ruhi is thankful to CSIR for her RA fellowship.

Author details

Gazala Ruhi and S.K. Dhawan

Polymeric & Soft Materials Section, National Physical Laboratory, (CSIR), Dr. K.S. Krishnan Marg, New Delhi, India

References

- [1] Wan Nik W B, Zulkifli F, Rahman M M and Rosliza R. International Journal of Basic & Applied Sciences 2011; 11, 75.
- [2] Jason L, Richard R, Edward L, Alexander F and Brenda L. Biofouling 2004; 20, 237.
- [3] Hernandez L A, Hernandez L S and Rodriguez-Reyna S L. International Journal of Corrosion 2012; 2102, 1.
- [4] Hanga T X, Truca T A, Olivierb M G, Vandermiersb C, Guéritc N and Pébèred N. Progress in Organic Coatings 2010; 69 (4) 410.
- [5] Shokry H. Chemistry of Metals and Alloys (2009); 2, 202.
- [6] Rani B E A, and Basu B B J. International Journal of Corrosion 2012; Review Article ID 380217, 15 pages.
- [7] Lee H and Neville K. Handbook of Epoxy Resins: Mc Graw Hill, New York; 1952.
- [8] Barletta M, Lusvarghi L, Mantini F P and Rubino G. Surface and Coatings Technology 2007; 20, 7479.
- [9] Yan M, Vetter C A and Gelling V J. Corrosion Science 2013; 70, 37.
- [10] Sharifirad M, Omrani A, Rostami A A and Khoshroo M. Journal of Electroanalytical Chemistry 2010; 645, 149.
- [11] Khanmohammadi M, Mizani F, Khaleghi M B, Garmarudi A B. Protection of Metals and Physical Chemistry of Surfaces 2013; 49 (6) 662.
- [12] Gergely A, Pfeifer E, Bertóti I, Török. T and Kálmán E. Corrosion Science 2011; 53 (11) 3486.
- [13] El-Shazly A H and Al-Turaif H A. International Journal of Electrochemical Science 2012; 7, 211.
- [14] Ohtsuka T. International Journal of Corrosion 2012; 1.
- [15] Al-Dulaimi A A, Hashim S and Khan M I. Pertanika Journal of Science and Technology 2011;19(2) 329.
- [16] Kousik G, Pitchumani S and Renganathan N G. Progress in Organic Coatings 2001; 43 (4) 286.
- [17] Sabouri M, Shahrabi T, Faridi H R and Salasi M. Corrosion Engineering Science and Technology 2009; 44 (1) 51.
- [18] Spinks G M, Dominis A J, Wallace G G and Tallman D E. Journal of Solid State Electrochemistry 2002; 6, 85.

- [19] Xu L, Chen W and Mulchandani A. *Angewandte Chemie International* 2005; 44, 6009.
- [20] Schaftinghen T V, Deslouis C, Hubin A and Terryn H. *Electrochimica Acta* 2001; 51, 1695.
- [21] Hien N T L, Garcia B, Pailleret A and Deslouis C. *Electrochimica Acta* 2005; 50, 1747.
- [22] Ferreira C A, Aeiya S, Coulaud A and Lacaze P C. *Journal of Applied Electrochemistry* 1999; 29, 259.
- [23] Troch-Nagels G, Winand R, Weymeersch A and Renard L. *Journal of Applied Electrochemistry* 1992; 22, 756.
- [24] Jassen W and Beck F. *Polymer* 1989; 30, 353.
- [25] Hulser P and Beck F. *Journal of Applied Electrochemistry* 1990; 20, 596.
- [26] Ferreira C A, Aeiya S, Aaron J J and Lacaze P C. *Electrochimica Acta* 1996; 41, 1801.
- [27] Pirvu C, Mindroiu M and Demetrescu I. *Key Engineering Materials* 2009; 415, 65.
- [28] Subathira A and Meyyappan R. *Recent Research in Science and Technology* 2010; 2(1) 124.
- [29] Liu A S and Oliveira M A S. *Materials Science-Poland* 2009; 27 (1) 265.
- [30] Raotole P, Patil P P and Raotole M. *International Journal of Emerging Technology and Advanced Engineering* 2013; 3 (11) 62.
- [31] Sathiyarayanan S, Azim S S and Venkatachari G. *Electrochimica Acta* 2007; 52, 2068.
- [32] Niedbala J. *Bulletin of Material Science* 2011; 34 (4) 993.
- [33] Herrasti P, Kulak A N, Bavykin D V, Ponce de Léon C, Zekonyte J, Walsh F C. *Electrochimica Acta* 2011; 56 (3) 1323.
- [34] Feng X M, Yang G, Xu Q, Hou W H and Zhu J J. *Macromolecular Rapid Communications* 2006; 27, 31.
- [35] Riaz U, Ashraf S M and Ahmad S. *Progress in Organic Coatings* 2007; 59, 138.
- [36] Qi K, Chen Z, Zhang G and Guo X. *The Open Corrosion Journal* 2011; 4, 18.
- [37] Lenz D M, Delamar M and Ferreira C A. *Journal of Electroanalytical Chemistry* 2003; 540 35.
- [38] Hosseini M G, Sabouri M and Shahrabi T. *Progress in Organic Coatings* 2007; 60 (3) 178.
- [39] Hosseini M G, Sabouri M and Shahrabi T. *Materials and Corrosion* 2006; 57 (5) 407.

- [40] Kumar S A, Bhandari H, Sharma C, Khatoon F and Dhawan S K. Polymer International 2012; 4066.
- [41] Al-Dulaimi A A, Shahrir H and Khan M I. Sains Malaysiana 2011; 40 (7) 757.
- [42] Marjanovic G C, DragicQevic L, Milojevic M, Mojovic M, Mentus S, DojcQinovic B, Marjanovic B and Stejskal J. Journal of Physics and Chemistry B 2009; 113, 7116.
- [43] Kin S H, Ahn S H and Hirai T. Polymer 2003; 44, 5625.
- [44] Dominis A, Spinks G M and Wallace G.G. 56th Annual Technical Conference on Society of Plastic Engineers 1998; 1229.
- [45] Shi H, Liu F, Yang L and Han E. Progress in Organic Coatings 2008; 62, 359.
- [46] Li H, Zhang Z, Ma X. Hu M, Wang X and Fan P. Surface and Coatings Technology 2007; 201, 5269.
- [47] Armelin E, Pla R, Liesa F, Ramis X, Iribarren J.I. and Aleman C. Corrosion Science 2008; 50, 721.
- [48] [48]Radhakrishnan S, Sonawane N and Siju C R. Progress in Organic Coatings 2009; 64, 383.
- [49] Saravanan K, Sathiyarayan S, Muralidharan S, Azim S and Venkatachari G. Progress in Organic Coatings 2007; 59, 160.
- [50] Srinivasaa P C and Tharanathana R N. Food Reviews International 2007; 23 (1) 53.
- [51] Portes E, Gardrat C, Castellan A and Coma V. Carbohydrate Polymers 2009; 76, 578.
- [52] Gupta B, Saxena S, Arora A and Alam M S. Indian Journal of Fibre and Textile Research 2011; 36, 272.
- [53] Liu B S, Huang T B, Yao C H, Fang S S and Chang C J. Journal of Medical and Biological Engineering 2009; 29, 60.
- [54] Sugama T and Cook M. Progress in Organic Coatings 2000; 38, 79.
- [55] Lu X, Wiren A and Albertson A. Proceedings of ACS Division of Polymeric Material: Science and Engineering 1998; 79, 242.
- [56] Vathsala K, Venkatesha T V, Praveen B M and Nayana K O. Engineering 2010; 2, 580.
- [57] Carneiro J, Tedim J, Fernandes S C M, Freire C S R, Gandini A, Ferreira M G S and Zheludkevich M L. Surface and Coatings Technology 2013; 226, 51.
- [58] Rath P C, Singh B P, Besra L and Bhattacharjee S. Journal of American Ceramic Society 2102; 95 (9) 2725.
- [59] Cordero-Arias L, Cabanas-Polo S, Gao H, Gilabert J, Sanchez E, Roether J A, Schubert D W, Virtanene S and Boccaccinia A R. RSC Advances; 2013; 3, 11247.

- [60] Ahmed R A, Farghali R A and Fekry A M. International Journal of Electrochemical Science 2012; 7, 7270.
- [61] Redepenning J, Venkataraman G, Chen J and Stafford N. Journal of Biomedical Material Research 2003; 66A, 412.
- [62] Yeh J M, Chin C P and Chang S. Journal of Applied Polymer Science 2003; 88, 3264.
- [63] Sugama T and Jimenez S M. Journal of Material Science 1999; 34, 2003.
- [64] Bumgardner J D, Wiser R and Gerard P D. Journal of Biomedical Science, Polymer Edition 2003; 14, 423.
- [65] Hahn B D, Park D S, Choi J J, Ryu J, Yoon W H, Choi J H, Kin H E and Kim S G. Surface and Coatings Technology 2011; 205 (8-9) 3112.
- [66] Yang S, Tirmizi S A, Burns A, Barney A A and Risen W M. Synthetic Metals 1991; 32, 191.
- [67] Khor E and Whey J L H. Carbohydrate Polymers 1995; 183.
- [68] Yang X and Lu Y. Polymer 2005; 46, 5324.
- [69] Yingmei L, Guicun L, Hongrui P and Kezheng C, Polymer International 2011; 60, 647.
- [70] Yalcinkaya S, Demetguil M, Timur V and Colk N. Carbohydrate Polymers 2010; 79 (4) 908.
- [71] Gacrielli G and Keddam V. Corrosion 1992; 48, 794.
- [72] Walter G W. Corrosion Science 1991; 32, 1041.
- [73] Wang J H, Duh J G and Shih H C. Surface and Coatings Technology 1996; 78, 248.
- [74] Singh I B. Corrosion Science 2003; 45, 2285.
- [75] Moutarlier V, Gigandet M P, Normand B and Pagetti J. Corrosion Science 2005; 47, 937.
- [76] Souto R M, Laz M M and Ries R L. Biomaterials 2003; 24, 4213.
- [77] Patil R N, Sharma B V and Mahanwar P A. Der Chemica Sinica 2012; 3 (2) 458.
- [78] Liu X P, Zheng T L and Xiong J P. International Journal of Electrochemical Science 2013; 8, 11588.
- [79] Manohar A K, Bretschger O, Nealsen K H and Mansfeld F. Bioelectrochemistry 2008; 72, 149.
- [80] Tsai C H and Mansfeld F. Corrosion Science 1993; 49, 726.
- [81] Nocodemo L. Corrosion 1993; 49, 235.
- [82] Grundmeier G, Schmidt W and Stratmann M. Electrochimica Acta 2000; 45, 2515.

- [83] Kending M and Scully J. Corrosion 1990; 46, 22.
- [84] Ruhi G, Bhandari H and Dhawan S K. (Communicated to) Surface and Coatings Technology, 2013.
- [85] Radhakrishnan S, Sonawane N and Siju C R. Progress in Organic Coatings 2009; 64, 383.
- [86] Saravanan K, Sathiyarayanan S, Muralidharan S, Azim S S and Venkatachari G. Progress in Organic Coatings 2007; 59, 160.
- [87] Fu Y, Su Y S and Manthiram A. Journal of Electrochemical Society 2012; 159 (9) 1420.
- [88] Lei J, Liang W and Martin C R. Synthetic Metals 1992; 48, 301.
- [89] Cheah K, Forsyth M and Truong M V. Synthetic Metals 1998; 94, 215.
- [90] Dai T, Yang X and Lu Y. Material Letters 2007; 61, 3142.
- [91] Chandrakanthi R L N and Careem M A. Thin Solid Films 2002; 417, 51.
- [92] Bose S, Kuila T, Uddin M E, Kim N H, Lau A K T and Lee J H. Polymer 2010; 48, 5921.
- [93] Zhang W H, Fan X D, Tian W and Fan W W. eXPRESS Polymer Letters 2012; 6 (7) 532.
- [94] Alam A, Sherif S M and Al-Zahrani S M, International Journal of Electrochemical Science 2013; 8, 3121.
- [95] Iroh J O and Su W. Electrochimica Acta 2000; 46, 15.
- [96] Wesseling B. Synthetic Metals 1997; 85, 1313.
- [97] Sathiyarayanan S, Muthukrishnan S and Venkatachari G. Progress in Organic Coatings 2006; 55, 5.
- [98] Nguyen T D, Nguyen T A, Pham M C, Piro B, Normand B and Takenouti H. Journal of Electroanalytical Chemistry 2004; 572, 225.
- [99] Bhandari H, Kumar S A and Dhawan S K. (2012), Conducting Polymer Nanocomposites for Anticorrosive and Antistatic Applications, Nano Composites-New Trends and Developments, In Tech Publishers, Croatia.
- [100] Creus j, Mazille H and Idrissi H. Surface and Coatings Technology 2000; 130, 224.
- [101] Shinde V, Sainkar A R and Patil P P. Corrosion Science 2005; 47,1352.
- [102] Pebre N, Picaud T, Duprat M and Dabosi F. Corrosion Science 1989; 29, 1073.
- [103] Ruhi G, Modi O P, Sinha A S K and Singh I B. Corrosion Science 2008; 50, 639.
- [104] Ruhi G, Modi O P and Singh I B. Surface and Coatings Technology 2009; 204, 359.

- [105] Ruhi G, Modi O P and Singh I B. Corrosion Science 2009; 51, 3057.
- [106] Loveday D, Peterson P and Rodgers B. Journal of Coatings Technology 2004; 1 (10) 88.
- [107] Metikos-Hukovic M, Tkalec E, Kwokal A and Piljac J. Surface and Coatings Technology 2003; 165 40.
- [108] Belluci F and Nicodemo L. Corrosion 1993; 49 235.
- [109] Zheludkevich M I, Shchukin D G, Yasakau K A, Mohwald H and Ferreira M G S. Chemistry of Materials 2007; 19, 402.
- [110] Rosero-Navarro M C, Pellice S A, Duran A and Apricio M. Corrosion Science 2008; 50, 1283.
- [111] Ruhi G, Dhawan S K. (Communicated to) Progress in Organic Coatings, 2013.
- [112] Modrzejewska Z, Stawczyk J, Matyka K, Matyka M, Mróz I and Ciszewski A. Polish Journal of Environmental Studies 2006;15 (4A) 84.
- [113] Thongnam M and Mc Clements D J. Langmuir 2005; 21, 79.
- [114] Vikhoreva G A, Babak V G, Galich E F and Galbraikh G S. Polymer Science A 1997; 39, 617.
- [115] Zhang H, Zhong X, Xu J. J and Chen H.Y. Langmuir 2008; 24, 13748.
- [116] Li X, Wan M, Wei Y, Shen J and Chen Z. Journal of Physics and Chemistry B 2006; 110, 14623.
- [117] Yoon H and Jang J. Advanced Functional Materials 2009; 19, 1567.
- [118] Yang X, Dai T and Lu Y. Polymer 2006; 47 (1) 441.
- [119] Marguerite R. Progress in Polymer Science 2006; 31, 603.
- [120] Aimoli C G, Torres M A and Beppu M. Material Science and Engineering C 2006; 26, 78.
- [121] Sakurai K, Maegawa T and Takahashi T. Polymer 2000; 41, 7051.
- [122] Zeng M, Fang Z and Xu C. Journal of Membrane Science 2004; 230, 175.
- [123] Zheludkevich M L, Serra R, Montemor M F, Yasakau K A, Salvado I M and Ferreira M G S. Electrochimica Acta 2005; 51 (2) 208.
- [124] Scully J R. Journal of Electrochemical Society 1989; 136 (4) 979.

